Review article

Enhanced sensing performance of ZnO nanostructures-based gas sensors: A review

Vijendra Singh Bhati [a], Mirabbos Hojamberdiev [b], Mahesh Kumar [c,*]

[a] Department of Physics, Indian Institute of Technology Jodhpur, 342011 Jodhpur, India
[b] Fachgebiet Keramische Werkstoffe, Institut für Werkstoffwissenschaften und -technologien, Technische Universität Berlin, Hardenbergstraße 40, 10623 Berlin, Germany
[c] Department of Electrical Engineering, Indian Institute of Technology Jodhpur, 342011 Jodhpur, India

ARTICLE INFO

ABSTRACT

Metal oxide semiconductors-based gas sensors have been extensively explored due to their high sensing response, cost-effectivity, long-term stability, and simple fabrication. However, their utilization at low operating temperature is still challenging. Thus, reduction in power consumption is highly essential for long-term usage of gas sensors. ZnO nanostructures-based gas sensors are one of the most eligible candidates where a real-time detection of explosive and toxic gases is needed. On this subject, numerous efforts have been made to improve the sensing response at reduced working temperature with the assistance of various methods. In this report, several techniques related to the synthesis of ZnO nanostructures and their efficient performance in sensing are reviewed. The report primarily focuses on different means of improving the sensing properties, such as functionalization of noble metal nanoparticles, doping of metals, inclusion of carbonaceous nanomaterials, using nanocomposites of different MO_x, UV activation, and post-treatment method of high-energy irradiation on ZnO nanostructures, with their possible sensing mechanisms. This study will therefore shed light on future proposals of ZnO-based gas sensors showing high sensitivity even at low operating temperature.

Contents

1. Introduction

Rapid expansions of industrialization and growing population in cities have resulted in air pollution. This pollution is mainly attributed to by-products of factories and automobile's exhaust which have created a major survival problem for living beings. Therefore, there is an urge for clean air supply to maintain our ecosystem. On the other hand, leakages of explosive and flammable gases are extremely dangerous for human beings and their belongings (Hübert et al., 2011). Hence, accurate real-time gas monitoring devices/sensors are highly essential, which also protect the environment and human beings within timely. Nowadays, gas sensors have become more popular because of

* Corresponding author.
　E-mail address: mkumar@iitj.ac.in (M. Kumar).

their various applications in fuel cells (for the detection of hydrogen gas), in mining industries (for the detection of methane), in automobile industries (for the detection of NO_2 from vehicle exhaust), in oil refineries (for the detection of hydrocarbons), and in fertilizer industries (for the detection of ammonia) (Sansone, 1992; Bhattacharyya et al., 2007; Wales et al., 2015; Wetchakun et al., 2011; Ghosh et al., 2013). Thus, a cost-effective, reliable, low power consuming, highly sensitive, and small size gas sensor is the most effective candidate to avoid unexpected situations caused by toxic and explosive gases (Özgür et al., 2005; Dey, 2018). Last few decades have witnessed an immense exploration of metal oxide (MO_x) semiconductor-based gas sensors which have excellent properties of an ideal gas sensor (Hahn et al., 2003; He et al., 2003; Korotcenkov et al., 2004; Shouli et al., 2010).

Recently, the development of nanostructured materials has resulted in enhanced gas sensing performance as compared to bulk material due to their superior qualities like large surface area and small size (Wang, 2008; Li et al., 2009). Till now, several types of MO_x-based gas sensors have been explored, including SnO_2, TiO_2, ZnO, WO_3, CuO, and Fe_2O_3 with different morphologies (Zhang et al., 2018a,b,c; Dwivedi et al., 2017; Vallejos et al., 2018; Urasinska-Wojcik et al., 2017; Umar et al., 2017; Sun et al., 2012). The sensing response of gas sensor usually depends upon the dimension of nanostructures (Choi and Jang, 2010; Liao et al., 2007a,b). Thus, several synthesis methods (for producing different nanostructures), including chemical vapor deposition, radio frequency (RF) sputtering, hydrothermal, electrospinning, sol–gel method, template synthesis method, molecular beam epitaxy, and metal organic chemical vapor deposition have been explored (Ameen et al., 2012; Baratto, 2018; Yang et al., 2013; Mondal and Sharma, 2016; Sui and Charpentier, 2012; Boyjoo et al., 2016; Ogata et al., 2001; Niu et al., 2018). Different types of morphologies and nanostructures can be achieved by using different types of synthesis methods. These nanostructures include thin films, nanoplates, nanospheres, nanowires, nanorods, nanotubes, nanoflowers, nanofibers, nanoneedles, and nanoribbons (Nunes et al., 2019). Hence, the detection of different target gases (both oxidizing and reducing), such as NH_3, NO_2, H_2, H_2S, SO_2, CO_2, CH_4, acetone, toluene, ethanol, and CO is made possible using different types of morphologies of MO_x-based sensors (Wang et al., 2010a,b).

Among all these MO_x sensors, ZnO-based gas sensors are broadly employed in various applications due to their excellent sensing response, good selectivity, easy fabrication, low cost, good thermal and chemical stability, and non-toxicity. Further, ZnO is intrinsically *n*-type semiconductor having a band gap of 3.37 eV, and a large exciton binding energy of 60 meV (Rai et al., 2012; Zheng et al., 2009). Apart from the gas sensing applications, ZnO nanostructures have been widely used in photovoltaic devices as well. Xu et al. (2011) reported the electropolymerized P3HT on vertically aligned thienylsilane-modified ZnO nanowires and observed that the polymerization onset potential was decreased for surface modified with thienylsilane groups of ZnO nanowires than the pristine ZnO nanowires. Venkatesan et al. (2015) showed the polymer/ZnO based hybrid solar cell with improved device lifetime. They synthesized bilayer interfaces of ZnO films with cationic polymer modification (PEIE) and found that the increased device lifetime for PEIE modified ZnO as compared to pristine ZnO film. Xu et al. (2011) reviewed the evolution of polymer–inorganic hybrid solar cells and described the mechanism, cell characterization, efficiency analysis of polymer–inorganic solar cells, and different approaches available to enhance the cell performance. Kumar et al. (2018) deposited Al doped ZnO (AZO) thin film by RF superimposed DC sputtering process. They utilized different RF/(RF + DC) ratios with same power and studied optical, structural, electrical and nanoscale grain boundaries potential. The results showed that the AZO film at the ratio of

0.75, exhibited low residual stress, high electron mobility and large crystallite size as compared to other AZO thin films. Wu et al. (2018a,b) reported the ZnO nanorod array based polymer-inorganic hybrid solar cells (HSCs) and TiO_2 nanorods array based polymer-inorganic HSCs and their performances were compared systematically. Efficiencies of ZnO nanorods based polymer HSCs was found lower than the TiO_2 nanorods based polymer HSCs and that was attributed to lower short-circuit current density of the ZnO nanorods based devices. Ngo et al. (2014) fabricated the polymer photovoltaic having ZnO as an electron transport layer and hole transport layer. The fabrication of device were utilized fully solution-processed (spin or spray coating) involving top electrode, hole transport layer and electron transport layer and then the device performance were compared with the solar cell whose top electrode was fabricated using thermal evaporator. They claimed that the similar device efficiencies were found using both techniques and the device fabrication cost can be reduced for large-scale production using airbrush rather than thermal evaporator for top metal electrode fabrication. Xie et al. (2010) investigated the electrolyte effects in electron transport and recombination at ZnO nanorods in dye-sensitized solar cells and suggested that the improved electron transport, reduced collection time, increased electron lifetime, suppressed charge recombination at the interface of ZnO nanorods/electrolytes when using different electrolyte. Xu et al. (2013) studied the organic (poly(3-hexylthiophene) or P3HT)-inorganic (ZnO) hybrid solar cells. Different ZnO nanostructures were grown such as nano-ridge and nanorods for electron acceptors/transporters and P3HT act as light absorber and electron donor. It was observed that the ZnO nanorod/P3HT ordered heterojunction devices shown excessive efficiency than the bilayer cells led to increased photocurrent which was caused by larger interface area of P3HT/ZnO.

ZnO have some advantages over other MOx based gas sensors such as its low cost and non-toxicity in nature that makes it eco-friendly. As ZnO is a chemoresistive sensor, the change in its resistance is highly depended on the presence of chemisorbed oxygen ions. In addition, the oxygen molecules are adsorbed on the surface of ZnO in presence of atmospheric air. Their formation thus occurs due to the extraction of electrons from the conduction band of ZnO which increases the resistance of ZnO. When reducing gases interact with the chemisorbed oxygen ions on the surface of ZnO, the reduction in resistance takes place because oxygen ions donate free electrons to the conduction band of ZnO. Furthermore, the sensing response of ZnO-based gas sensor is significantly affected by the working temperature and gas concentration (Kumar et al., 2017). The dependency of ZnO-based gas sensors with working temperature usually requires sufficient thermal or light energy on the surface of sensor so that the activation energy barrier is surpassed for the enhancement of the redox reaction, further enhancing the sensing response (Ranwa et al., 2014; Xu and Ho, 2017). However, there are some trade-off conditions with regard to enhanced sensing response at high working temperature. Not only this, the surface morphologies of ZnO nanostructures change at high operating temperature. It was also found that the sensing response of the sensor reduces due to the reduction of chemisorbed oxygen ions on the surface above optimum operating temperature (Jing and Zhan, 2008). Keeping the concern for power in mind, the working temperature for a gas sensor is kept as low as possible. Thus, the need for the enhancement in sensing response, fast response time, long-term stability, selectivity, and reproducibility at low working temperature has paved advanced method for the modification of ZnO nanostructures. A few techniques of improving the gas sensing properties of ZnO include doping of metals into ZnO, functionalization of noble metal nanoparticles on the surface of ZnO, compositing ZnO with other metal oxides, UV activation,

high energy irradiation on ZnO nanostructures, and inclusion of carbonaceous nanomaterials into ZnO (Zhang et al., 2018a,b,c; Lupan et al., 2018; Yang et al., 2019; Wu et al., 2018a,b; Kim et al., 2019a,b,c; Barthwal et al., 2017; Bhati et al., 2018a,b).

To the best of our knowledge, enormous study has been done on ZnO-based gas sensors (Seiyama et al., 1962; Zeng et al., 2015; Das and Sarkar, 2017; Ganesh et al., 2017). However, only a few of them deal with a review on ZnO-based gas sensors focusing all possibilities to improve the gas-sensing properties and highlight their gas-sensing mechanisms (Kumar et al., 2015; Zhu and Zeng, 2017). In view of further modification of these sensors for improving the sensing properties, in this minireview, we present a brief review of the latest reports on various techniques available for the synthesis of ZnO nanostructures, effect of metal doping, functionalization of noble metal nanoparticles, inclusion of carbonaceous nanomaterials, nanocomposite of MO_x, UV activation, e-beam irradiation, etc. Also, the gas sensing mechanisms will be discussed in brief, and future aspects of ZnO-based gas sensors are summarized.

2. Synthesis of ZnO nanostructures

Several methods have been previously applied for the synthesis of ZnO nanostructures. Namely, chemical vapor deposition, RF sputtering, hydrothermal, electrospinning, sol–gel, template synthesis method, molecular beam epitaxy, and metal–organic chemical vapor deposition were used to synthesize different morphologies and sizes of ZnO nanostructures (1-D, 2-D, and 3-D). Among them, the 1-D nanostructures, such as nanowires, nanorods, nanofibers, nanoneedles, nanoribbons, and nanotubes form the biggest group. The 2-D nanostructures include nanosheets and nanoplates, while nanoflowers, dendrimers, and urchins are the example of 3-D nanostructures.

Chemical vapor deposition (CVD) is based on vapor transfer and deposition on the substrate. The growth of nano- and microstructures occurs on a heated substrate in the form of vapor during the chemical reaction process. The key parameters for the deposition of ZnO nanostructures by CVD generally depend upon the substrate position, growth temperature, deposition time, gas flow rate, and pressure (Yang et al., 2016). However, the adjustment in deposition parameter with proper optimization leads to the growth of different sizes and shapes of nano- and microstructures. Many reports have shown that the use of metal catalyst on the substrate surface increases the chances of growing the 1-D nanostructures by CVD. This possible growth mechanism is known as vapor–liquid–solid (VLS) method (Solís-Pomar et al., 2011). For instance, Babu and Hong (2015) studied the deposition over ZnO nanorods. That is, prior to the growth of nanorods, a 200-nm thick ZnO seed layer was deposited on a silicon substrate so that the seed layer facilitates the nucleation of ZnO nanorods on the silicon substrate. Tuayjaroen and Jutarosaga (2017) grew 1-D and 2-D ZnO microstructures on an ITO/borosilicate glass substrate by oxygen-assisted thermal CVD and claimed that the transition from 1-D to 2-D microstructures was due to the increase of supersaturation in vapor — solid growth mechanism with increasing oxygen partial pressure.

Radio frequency (RF) sputtering is another efficient technique to fabricate ZnO nanostructures on the desired substrate. Excellent adhesion and uniformity throughout the substrate make it the most advantageous technique for the deposition of ZnO nanostructures. The basic principle of sputtering is based on the ejection of atoms from the source material, and deposition on the substrate. The deposition process runs in plasma where argon is the process gas. Sputtering process mainly depends upon the RF power, substrate temperature, argon flow, target to substrate distance, and gas pressure. Most of the literature survey report

ZnO thin films using RF sputtering technique. However, a few studies have also investigated the fabrication of ZnO nanorods by RF sputtering. Ranwa et al. (2014) have grown vertically aligned ZnO nanorods without using any metal catalyst on the substrate by RF magnetron sputtering system. The growth parameters, such as substrate temperature, chamber pressure, Ar gas flow rate, RF power, and substrate to the target distance were taken to be 500 °C, 2×10^{-2} mbar, 60 sccm, 150 W, and 14 cm, respectively.

Another synthesis method for the ZnO nanostructures is hydrothermal route where the growth of ZnO nanostructures occurs in an autoclave at lower temperature as compared to other synthesis techniques. However, the growth of ZnO nanostructures requires more time than other techniques. Finally, the formation of a nucleation site leads to the growth of nanostructures. This method has several benefits, such as low temperature requirement for growth, low cost, different dimensions and shapes of nanostructures relying on the composition of materials, different pressure as well as high crystallinity (Tam et al., 2006; Baruah and Dutta, 2009; Cho et al., 2006). Umar et al. (2012) presented flower-shaped ZnO nanostructures grown by hydrothermal process using zinc nitrate hexahydrate, hexamethylenetetramine (HMTA), and sodium hydroxide (NaOH) in autoclave at 145 °C for 3–7 h. Furthermore, electrospinning technique is widely used to synthesize 1-D nanostructures, particularly nanofibers and nanotubes with an extended length, which have an equally distributed diameter along the length and high surface area. This technique is relatively simple and cost-effective, allowing synthesizing various nano- and micro-scaled materials (Guo et al., 2010). The working principle of electrospinning is that an electric field is applied between the capillary tube (normally used as syringe) and the collector (aluminium plate), resulting in the as-spun nanofibers. These nanofibers have to be collected from the collector surface, and the final product is obtained after calcination process. Here, the syringe contains metal ions polymeric solution of the desired material. On similar lines, Wei et al. (2011) synthesized ZnO hollow and solid nanofibers via single capillary electrospinning.

Sol–gel method involves the hydrolysis or alcoholysis of the precursor dissolved in solvents. The formation of sol is due to hydrolysis or alcoholysis, and the process of recondensation, and aging is responsible for the formation of gel. Subsequently, the materials undergo drying, sintering, and other process as per the requirement of nanostructures (Znaidi, 2010). Usually, the precursor materials are metal salts or inorganic salts. Kim et al. (2017) fabricated ZnO thin film using sol–gel method.

Template method is also used to fabricate ZnO nanostructures. In this method, a template with predefined size and shape utilizes the growth of nanostructures through the pores or channel of template via nucleation and growth process. There are two types of templates, such as hard and soft template. A hard template usually involves CNT and porous alumina, while a soft template comprises of flexible polymer, biomolecular, and single molecular-based template. Zhang et al. (2013) synthesized ZnO hollow spheres using bacterial template method. Zhou et al. (2018) have fabricated ZnO@ZIF core–shell structures using hydrothermal method, while two zeolitic imidazolate frameworks (ZIFs) with their different pore sizes (3.4 Å for ZIF-8, and 4.8 Å for ZIF-71) were coated on ZnO nanorods (acts as template for ZIF). Fig. 1(a–c) shows FESEM images of vertically aligned ZnO NRAs and ZnO@ZIF core shell structures. The deposition of ZnO nanostructures can also be performed by using molecular beam epitaxy (MBE). In this process, a molecular flow of Zn is sprayed onto the substrate in the presence of reactive oxygen. The entire deposition process is carried out in ultra-high vacuum chamber. However, the equipment and maintenance costs are high, and the growth speed is slow. Reshchikov et al. (2007) deposited
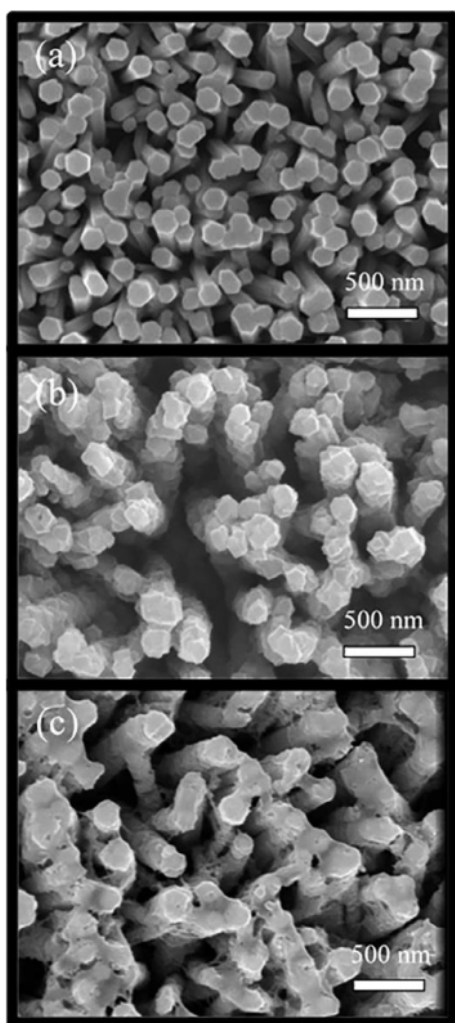
Fig. 1. SEM images of different ZnO NRAs: (a) vertically-aligned ZnO NRAs, (b) ZnO NRAs coated with ZIF-8, and (c) ZnO NRAs coated with ZIF-71. Copyright 2018, Elsevier.
Source: Reprinted from Ref. Zhou et al. (2018) with permission.

MBE-grown ZnO films on a sapphire substrate using H_2O_2 as a source of reactive oxygen. Another method known as metal organic chemical vapor deposition (MOCVD) is widely used to deposit ZnO nanostructures. Generally, metal organic compounds serve as source material, and the growth occurs via evaporation, reaction, and deposition process on the desired substrate.

Mohanta et al. (2008) fabricated well-aligned ZnO nanorods on *c*-sapphire substrate at 300 °C and 1 Torr pressure using MOCVD. Table 1 shows different types of ZnO nanostructures grown by various synthesis techniques.

3. Gas sensing mechanism

The gas sensing mechanism of ZnO nanostructures-based gas sensors relies on the alteration of a depletion layer on the surface of ZnO nanostructures. The oxygen molecules are adsorbed on the ZnO surface in the presence of atmospheric air. Furthermore, the formation of oxygen ions occurs on the surface due to the extraction of electrons from the conduction band of ZnO, leading to an increase in the resistance of ZnO. The mechanism can also be understood by band bending theory. The adsorption of oxygen ions on ZnO increases the band bending in upward

direction under atmospheric oxygen due to high electronegativity of oxygen molecules and increased the barrier height (Dey, 2018). Moreover, the adsorbed oxygen ions (O_2^-, O^-, and O^{2-}) are highly dependent on working temperature (Ranwa et al., 2014). In addition, UV light illumination on the ZnO surface can increase reaction kinetics at lower temperature as compared to thermally activated ZnO. When reductive gases, such as NH_3, H_2, HCHO, and CH_4, interact with chemisorbed oxygen ions on ZnO surface, there is reduction in resistance. This is because oxygen ions donate free electrons to the conduction band of ZnO and the barrier height decreases. On the other hand, the behavior of ZnO nanostructures towards oxidative gases, such as NO_2 and CO_2, is opposite to the behavior of the above-discussed reductive gases (Dey, 2018).

The modification in electrical behavior of thin film like structures is mainly caused by the grain boundaries, while the effect of electrical behavior in 1-D ZnO nanostructures usually takes place due to the entire surface (Xu et al., 2000a,b). Thus, high surface area and large depletion layer of 1-D ZnO nanostructures lead to a greater change in resistance as compared to ZnO thin films under exposure to target gases. Fig. 2(a–b) shows gas sensing mechanism for nanofibers, nanoplates, and nanoflowers for HCHO gas via UV activation at room temperature (Cui et al., 2016). The sensing response was the highest for nanofibers as their grain size was small. Therefore, the large change in the depletion layer occurred, as shown in Fig. 2(a). On the contrary, the particle sizes of nanoplates and nanoflowers were larger, leading to a small change in the depletion layer, indicating a lower sensing response as compared to nanofibers (Fig. 2(b)). However, change in barrier height was higher for nanofibers as compared to nanoplates and nanoflowers.

4. Efficient ways to improve the sensing response

The sensing response can be enhanced via metal doping into ZnO, functionalization of noble metal nanoparticles on ZnO surface, inclusion of carbonaceous nanostructures, composition of different MO_x nanostructures, UV activation, and e-beam irradiation. Here, we will discuss the above-mentioned effective ways to improve the sensing response with possible gas sensing mechanism.

4.1. Metal doping

Doping is one of the most important factors that increase the sensing response of ZnO nanostructures (Chang et al., 2014). Transition metals, such as Ni, Co, Fe and Cu, have been significantly used as dopants into ZnO nanostructures (Zhang et al., 2017a,b; Maswanganye et al., 2017; Bai et al., 2014; Gong et al., 2006). The dopants not only increase the activity, but also modify the resistance of ZnO. The dopants also reduce the working temperature of the sensor, improve its selectivity, stability, and fast response towards target gas (Bhati et al., 2018a,b). It has been observed that the surface morphology of ZnO nanostructures changes upon introducing the metal dopants (Iqbal et al., 2013). The particle size of doped ZnO nanostructures becomes smaller than pristine ZnO nanostructures due to the further restriction of the movement of crystallites when the boundaries between the dopant and the host material interact (Maciel et al., 2003). Thus, the crystal growth stops due to the introduction of dopant. Gas sensing can be improved because small-sized particles have high surface area which further increases the number of chemisorbed oxygen ions and barrier height. Bhati et al. (2018a,b) deposited Ni-doped ZnO nanostructures (0, 2, 4, 6% Ni) on silicon substrate.

It was observed that the morphology of densely packed nanorods of undoped ZnO was transformed into nanoplates for

Table 1
Types of ZnO nanostructures grown by different synthesis techniques.

| Type of ZnO nanostructures	Second material used	Deposition technique	Ref.
ZnO nanorods	Ni layer (10 nm) on ZnO nanorods	Chemical vapor deposition	Mudusu et al. (2016)
ZnO nanowires	Au thin film (∼0.5–3 nm) on substrate	Chemical vapor transport and condensation	Yang et al. (2002)
ZnO nanowires/nanorods	Zn seed layer on substrate	Chemical vapor deposition	Rodwihok et al. (2019)
ZnO nanorods	No catalyst used on silicon substrate	RF magnetron sputtering	Sundara Venkatesh et al. (2014)
ZnO:Al layers	2% Al_2O_3 doped with ZnO	RF magnetron sputtering	Zdyb et al. (2018)
ZnO nanorods	Seed layer of ZnO nanoparticles	Hydrothermal	Yatskiv and Grym (2016)
ZnO nanosheets	Al_2O_3 tube as substrate	Hydrothermal	Ju et al. (2014)
ZnO nanoflowers	Al_2O_3 substrate	Hydrothermal	Song et al. (2019)
Pure ZnO and Pr doped ZnO nanofibers	–	Electrospinning	Wang et al. (2014)
$ZnO/ZnCo_2O_4$ nanotubes	–	Electrospinning	Alali et al. (2017)
Co doped ZnO nanofibers	–	Electrospinning	Liu et al. (2011)
ZnO thin films	Soda-lime glass, SiO_2, Si, and Pt substrates	Sol–gel	Ayana et al. (2016)
ZnO thin films	Sapphire substrate	Sol–gel	Chia et al. (2013)
ZnO hierarchical Microstructure	Ceramic substrate	Sacrificial template method	Li et al. (2019)
ZnO quantum dots	–	Aptamer template	Kiruba Daniel et al. (2019)
ZnO nanobelts	Au coated sapphire substrate	MBE	Kennedy et al. (2018)
ZnO layers	Sapphire substrate	MBE	El-Shaer et al. (2005)
ZnO nanotips	r-plane sapphire substrate	MOCVD	Biswas et al. (2013)
ZnO thin film	Quartz substrates	MOCVD	Pati et al. (2013)
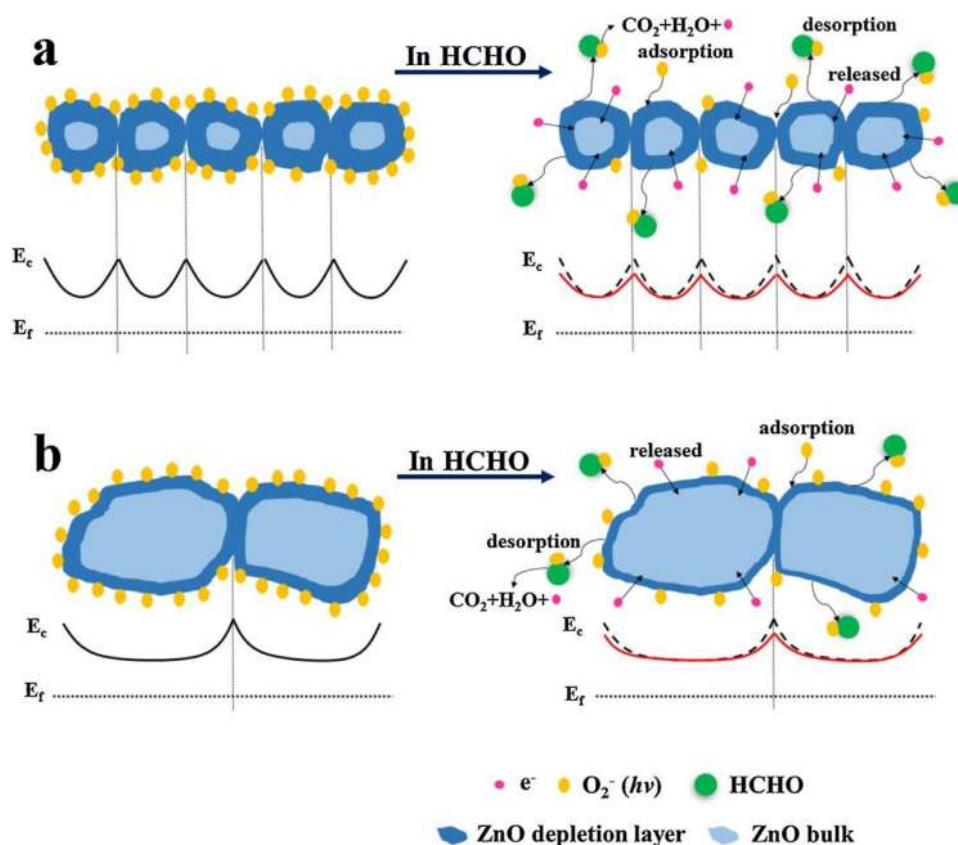
Fig. 2. Gas sensing mechanism of ZnO nanofibers under UV illumination: (a) ZnO nanoplates and (b) ZnO nanoflowers in the presence of HCHO. Copyright 2016, Elsevier.
Source: Reprinted from Ref. Cui et al. (2016) with permission.

Ni-doped ZnO, as can be seen in the FESEM images in Fig. 3(a–h). The relative response for 100 ppm H_2 gas at 150 °C was the highest for 4% Ni-doped ZnO nanostructures when compared to other samples (Fig. 3(i)). The enhanced sensing response was attributed to the lowest activation energy of 4% Ni-doped ZnO nanostructures and the presence of a large number of active sites for incoming H_2 gas. Apart from this, they also showed that 4% Ni-doped ZnO has high stability and good selectivity. Moreover, the substitution of Zn ions occurred in the ZnO lattice due to the replacement by dopant as the ionic radius of Zn is similar to that of dopant, and correspondingly creates donor defects. Sett and Basak (2017) prepared Co-doped ZnO (0, 2, 4, 6, 8% Co) nanorods on glass substrate by hydrothermal method.

The gas sensing response was analyzed for different concentrations of H_2 at 300 °C. It was observed that the highest sensing response was noted for 8% Co-doped ZnO nanorods, as shown in Fig. 4(a–b). The enhanced sensing response was due
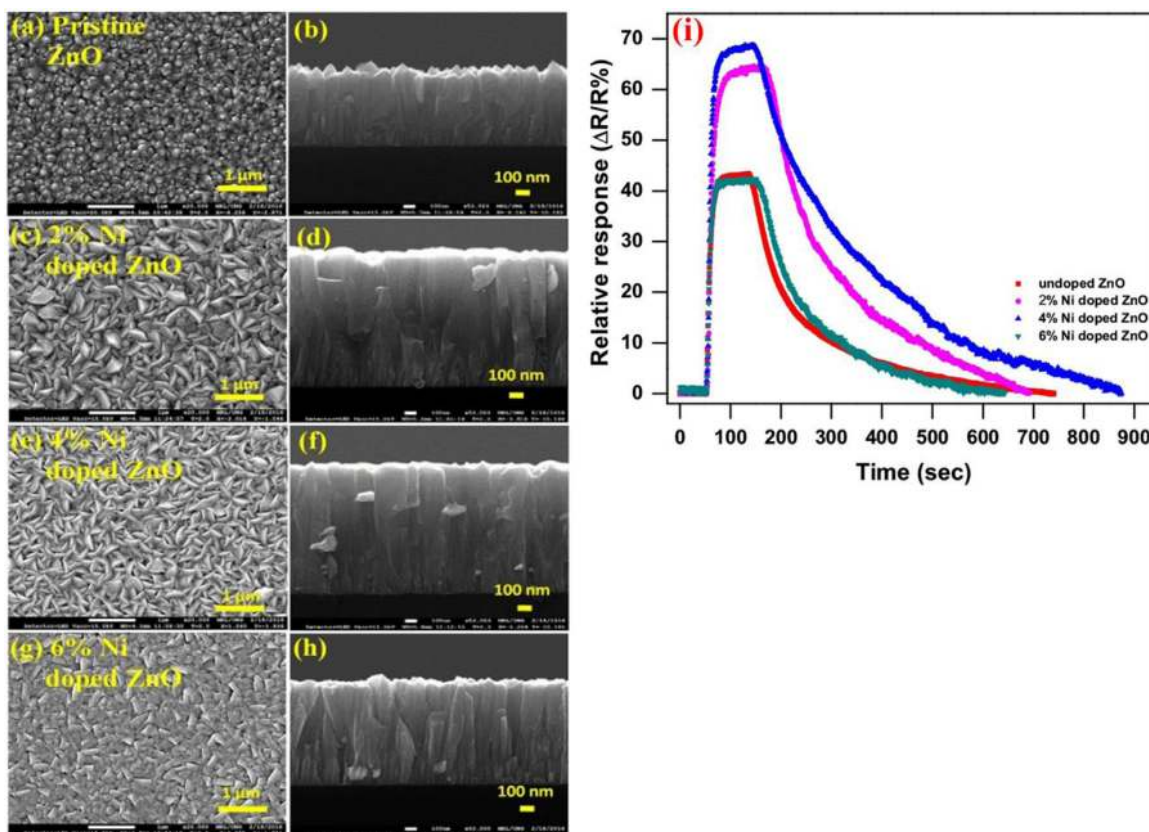
Fig. 3. FESEM images of (a, b) undoped, (c, d) 2% Ni-doped ZnO, (e, f) 4% Ni-doped ZnO, (g, h) 6% Ni-doped ZnO nanostructures, and (i) Relative response of undoped and Ni-doped ZnO for 1% H_2 at 150 °C.
Copyright 2018, Elsevier.
Source: Reprinted from Ref. Bhati et al. (2018a,b) with permission.

to high surface to volume ratio of nanorods and increased surface defects (oxygen vacancies) as depicted in Fig. 4(c). Other studies have also revealed that the sensing response can also be increased by the formation of *p-n* junction between *p*-type dopants (Ni, and Cr) and *n*-type ZnO nanostructures (Cheng et al., 2012; Wang et al., 2010a,b). Table 2 shows different metals-doped ZnO nanostructures-based gas sensors at different working temperatures.

4.2. Functionalization of noble metal nanoparticles

The gas sensing response can be enhanced via functionalization of noble metal nanoparticles (e.g., Pd, Pt, and Au) on the surface of ZnO nanostructures (Zhang et al., 2016; Kondalkar et al., 2019; Kim et al., 2019a,b,c; Li et al., 2008; Xu et al., 2000a,b; Ramgir et al., 2013). Two types of mechanisms are commonly used to describe the improved sensing response by functionalized noble metal nanoparticles on ZnO nanostructures. The first one is "*chemical mechanism*" and the second is "*electronic mechanism*". The chemical mechanism is based on the spill-over effect (Dey, 2018). The functionalized noble metal nanoparticles on ZnO nanostructures stimulate the adsorption and desorption process for oxygen molecules. When oxygen molecules interact with these noble metal nanoparticles, they are split into oxygen atoms and spread over the entire surface. Then, these oxygen atoms remove electrons from the conduction band of ZnO and convert themselves into the oxygen ions. Furthermore, the depletion layer is enhanced on the surface of ZnO, and the overall resistance of the sensor increases. When reductive gases are exposed on the sensor surface, they react with the catalytic nanoparticles and split on the ZnO surface. Therefore, a large

number of oxygen ions are available to react with the atoms of the reductive gas, and subsequently, there is a massive reduction in depletion layer as well as resistance of the sensor, and free electrons are released into the conduction band of ZnO. Hence, this effect not only reduces the working temperature of ZnO-based sensor, but also increases its sensing response and selectivity. In the case of electronic mechanism, a nano-Schottky junction is developed between the noble metal nanoparticles and ZnO because electrons are shifted to the nanoparticles because of their different work functions. Thus, band bending is created at the interface of noble metal nanoparticles and ZnO which further increases the resistance of the sensor and its depletion layer.

Kim et al. (2019a,b,c) synthesized Pt- and Pd-functionalized ZnO nanowires. The sensors were operated in self-heating mode for reduction in working temperature. It was shown that Pt-functionalized nanowires exhibited a maximum sensing response of around 2.86 for 50 ppm toluene, while Pd-functionalized nanowires showed a maximum sensing response of 2.20 for 50 ppm benzene at room temperature. The sensing mechanism was ascribed to the excellent catalytic behavior of Pt and Pd, leading to the formation of Schottky barrier that provides more adsorption sites on the sensor surface. Chen et al. (2019a,b) have grown ZnO nanowires by hydrothermal technique and functionalized them with Pd nanoparticles (0, 1, 2 and 5% Pd) so as to utilize them for NO_2 gas sensing, as can be seen in Fig. 5(a-d). The sensor showed a high sensing response ∼13.5 (R_a/R_g), and a fast response time for 1 ppm at 100 °C. The enhanced sensing mechanism was due to the synergistic effect of chemical and electronic mechanisms as shown in Fig. 5(e). Table 3 displays a comparison of gas sensing response based on functionalized noble metal nanoparticles/ZnO nanostructures at different temperatures.
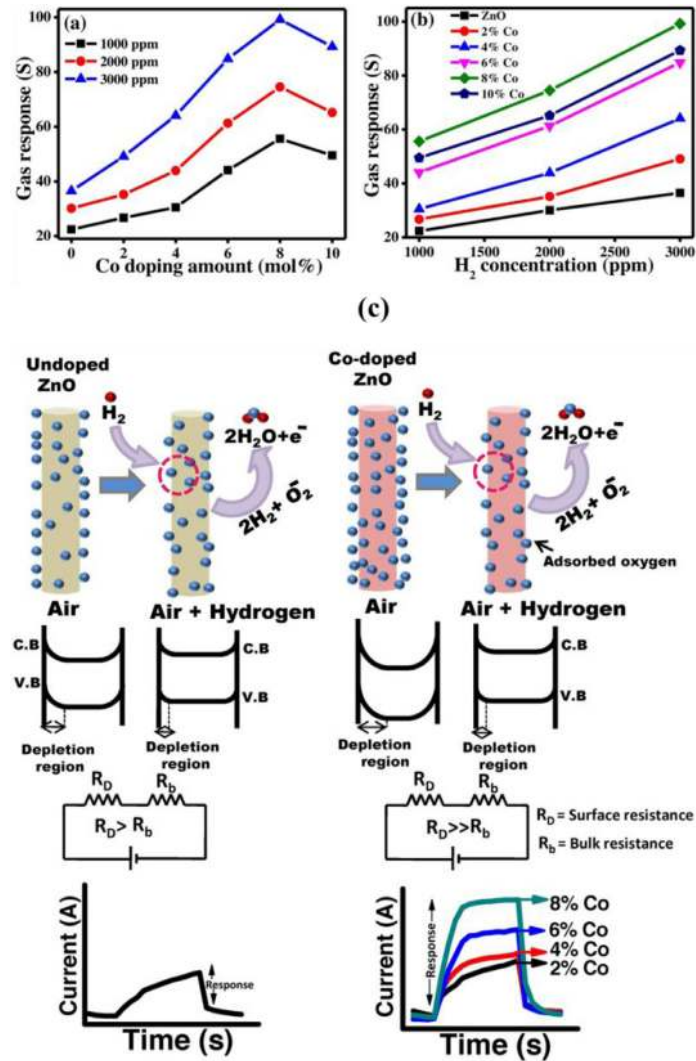
Fig. 4. (a) Gas response with different Co doping contents at 300 °C, (b) gas response of all sensors for different H_2 concentration at 300 °C, and (c) sensing mechanism of undoped and Co-doped ZnO NRs.
Copyright 2017, Elsevier.
Source: Reprinted from Ref. Sett and Basak (2017) with permission.

Table 2
Gas sensing response based on doped ZnO nanostructures at different temperatures.

| Dopant	Morphology	Synthesis (ZnO) method	Gas	Temp. (°C)	Sensing response	Res. time	Ref.
In	3-D ordered macroporous	Template method	Ethanol, 100 ppm	250	∼88 (R_a/R_g)	25 s	Wang et al. (2016)
Co	Nanowires	Thermal evaporation	p-xylene, 5 ppm	400	19.55 (R_a/R_g)	–	Woo et al. (2014)
Co	Thin film	Spray pyrolysis	NH_3, 100 ppm	RT	3.48 (R_a/R_g)	100 s	Mani and Rayappan (2015)
Ni	Nanorods	Hydrothermal	H_2S, 100 ppm	200	45.3 (R_a/R_g)	48 s	Modaberi et al. (2018)
Co	Hierarchical microspheres	Hydrothermal	1, 2-dichloroethane, 100 ppm	440	23.7 (R_a/R_g)	30 s	Zhu et al. (2012)
La	Bead	Electrospinning	Acetone, 200 ppm	340	64 (R_a/R_g)	16 s	Xu et al. (2015)
Cr	Nano-whiskers array	Spray pyrolysis	H_2, 400 ppm	RT	133 (R_a/R_g)	–	Renitta and Vijayalakshmi (2016)
Al	Nanoparticles	Fame spray pyrolysis (FSP)	Acetone, 10 ppm	450	245 (R_a-R_g)/R_g	3 s	Yoo et al. (2019)
Tb	Nanoparticles	Co-precipitation	Ethanol, 50 ppm	280	∼49 (R_a/R_g)	–	Hastir et al. (2016)
Ce	Nanoflower	Precipitation	Ethanol, 100 ppm	300	72.6 (R_a/R_g)	3 s	Chang et al. (2013)
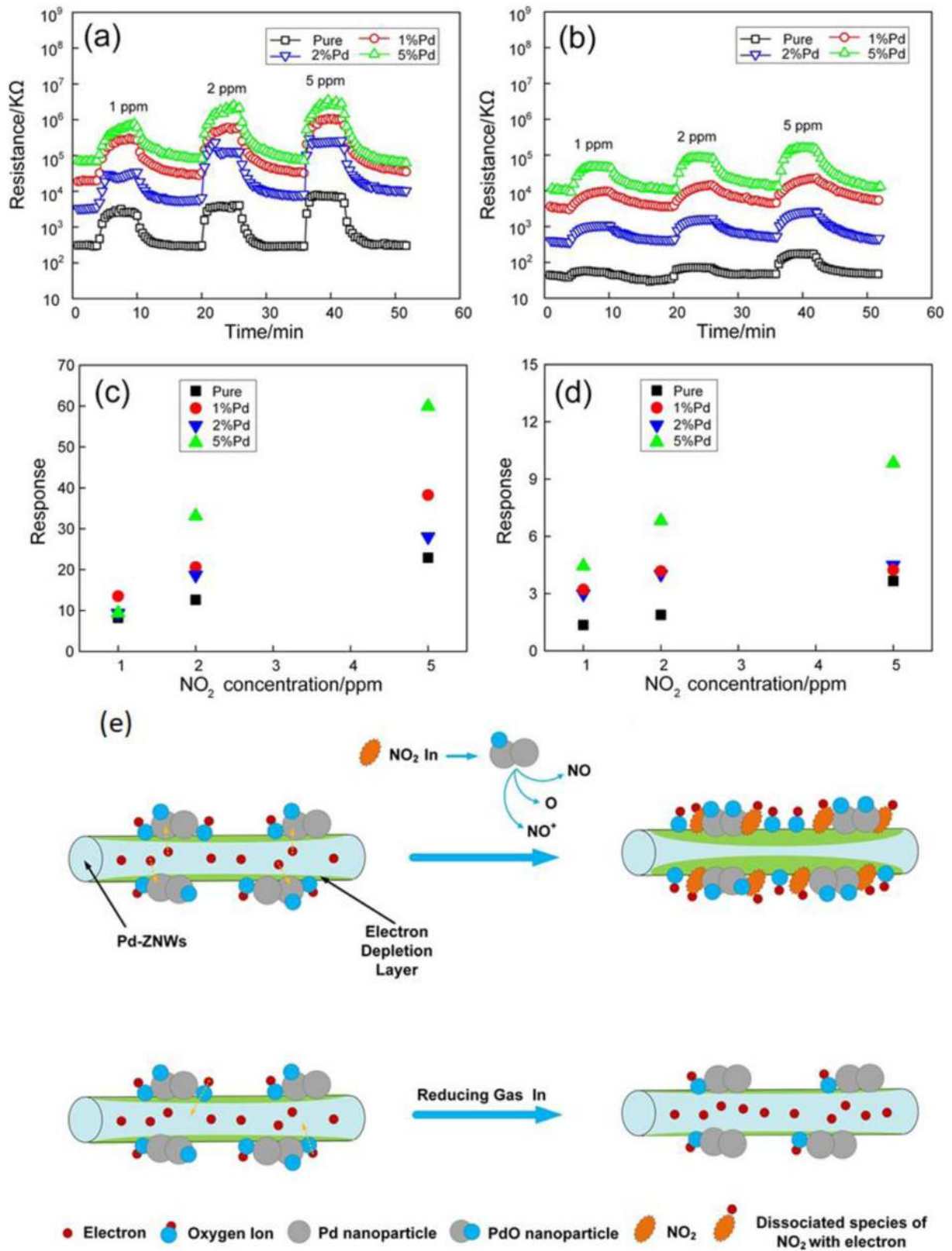
Fig. 5. Dynamic response of sensor under different concentrations of NO_2 for pure ZNWs (150 °C) and Pd-ZNWs (100 °C) at (a) 30% RH and (b) 60% RH and (c–d) corresponding sensor response at (c) 30% RH and (d) 60% RH. (e) Sensing mechanism for Pd-ZNWs under NO_2 and reducing gases.
Copyright 2019, Elsevier.
Source: Reprinted from Ref. Chen et al. (2019a,b) with permission.

Table 3
Gas sensing response based on functionalized noble metal nanoparticles/ZnO nanostructures at different temperatures.

Nanoparticles	Morphology (ZnO)	Synthesis method (ZnO)	Gas	Temp. (°C)	Sensing res.	Res. time	Ref.
Pd	Nanorod arrays	Photochemical	H_2, 500 ppm	260	1106 (R_a/R_g)	–	Chang et al. (2013)
Bimetallic Au/Pd	Nanowires	Hydrothermal and dipping	NO_2, 1 ppm	100	94.2 (R_g/R_a)	35 s	Chen et al. (2019a,b)
Au	Nanowires	Hydrothermal	Ethanol, 100 ppm	380	33.6 (R_aR_g)	3 s	Guo et al. (2014)
Ag	Hollow nanocages	Precipitation	Ethane, 100 ppm	250	84.6 (R_a/R_g)	5 s	Zhang et al. (2019)
Pt-Au bimetallic	Nanorods	Hydrothermal	H_2, 250 ppm	RT	25 (R_a/R_g)	115 s	Fan et al. (2017)
Au	Nanorods	Hydrothermal	CO, 1000 ppm	150	12 (R_a/R_g)	–	Rai et al. (2012)
Pd	Nanowires	VLS growth	CO, 0.1 ppm	RT	1.02 (R_a/R_g)	210 s	Choi and Kim (2012)
Pd	Nanowires	VLS growth	H_2, 100 ppm	350	87.17 (R_a/R_g)	–	Kim et al. (2019a,b,c)
Ag	3D microspheres	Precipitation	Triethylamine,	183.5	6043 (R_a/R_g)	1 s	Shen et al. (2018)

4.3. Inclusion of carbon-based nanomaterials

The combination of carbonaceous nanomaterials with ZnO nanostructures is the most efficient approach to improve the sensing response, with high selectivity, and fast response time (Xiao et al., 2018). There are several types of carbon materials, such as carbon nanofibers (1-D), carbon nanotubes (1-D), and graphene (2-D) and its derivatives. Pure graphene-based gas sensors are not commonly used because of the absence of functional groups and band gap. Thus, the attachment of functional groups on the surface of graphene is highly essential to tune the band gap and provide extra active sites to target gas molecules (Gupta Chatterjee et al., 2015). Among all carbon nanomaterials, reduced graphene oxide (rGO)/ZnO-based sensors have been extensively studied due to superior qualities like fast response, excellent sensing response and good selectivity.

The basic idea of enhancement in sensing response depends on the formation of a heterojunction between carbon materials and ZnO because they have different work functions and semiconducting properties. Another reason of enhancement is the nanoporous structure of carbon materials that diffuses the target gas molecules. Moreover, the presence of functionalized oxygen groups also provides some active sites to increase the sensing response. Abideen et al. (2015) proposed RGO nanosheets (0, 0.04, 0.11, 0.17, 0.44, 0.77, 1.04 wt% RGO)-loaded ZnO nanofibers via electrospinning method for NO_2 gas. All sensors were used to detect 5 ppm NO_2 at 400 °C. It was found that 0.44 wt% RGO-loaded ZnO-based sensors showed the highest sensing response (Fig. 6(a–b)).

The excellent sensing response was explained in Fig. 6(c–d) with the following reasons: (i) surface adsorption/desorption in the presence of air and NO_2; (ii) increased depletion layer due to the presence of ZnO/ZnO homointerfaces; (iii) formation of heterointerfaces between RGO (*p*-type) and ZnO (*n*-type) provides more adsorption sites for NO_2 gas; (iv) attachment of functional groups on RGO. Schütt et al. (2017) deposited ZnO-CNT hybrid tetrapods for NH_3 sensing. Firstly, ZnO tetrapodal networks were grown by flame transport synthesis process and CNT was attached to ZnO tetrapodal networks by a dipping method. They found that the highest sensing response of about 6.4 was achieved as compared to other sensors towards 100 ppm NH_3 at room temperature. Table 4 shows gas sensing response based on different carbon nanomaterials/ZnO nanostructures at different temperatures.

4.4. Nanocomposites with different MO_x

A homojunction is created between the particles in ZnO nanostructures, exhibiting the sensing response due to the ZnO-ZnO barrier height under the exposure of target gases. On the other hand, when two dissimilar MO_x are composited together with different values of work functions, electrons will flow from low work function of MO_x to high work function of MO_x until their Fermi levels become equal. Therefore, band bending occurs at the interface of two dissimilar MO_x, forming a heterojunction and leading to an increase in the overall resistance and barrier height. It has been observed that the nanocomposite of *p*-type and *n*-type nanostructures gives rise to barrier height due to a large difference in their work functions. When reductive or oxidative gases are exposed on these heterojunctions, enormous change in the resistance and depletion layer occurs (Han et al., 2019). Therefore, the sensing response of ZnO nanostructures can be enhanced using this technique.

Zhang et al. (2014) fabricated flower-like *p*-CuO (0, 0.125, 0.25, and 0.5)/*n*-ZnO heterojunction nanorods by hydrothermal technique, and their morphologies can be seen in FESEM images shown in Fig. 7(a–h). They showed that the highest sensing response was observed for 0.25:1 CuO/ZnO nanorod based sensor for 100 ppm ethanol at 300 °C. This sensing response was 2.5 times higher than ZnO-based sensor (Fig. 7(i)). The enhancement in sensing response was attributed to the formation of a heterojunction between *p*-type of CuO and *n*-type of ZnO, as shown in Fig. 7(j–k). Moreover, a large reduction in barrier height was noted under ethanol vapor. Katoch et al. (2015) have reported the SnO_2-ZnO composite nanofibers and detected 10 ppm H_2 at 300 °C. The enhanced sensing response for H_2 was because of the formation of the SnO_2-SnO_2 homointerfaces and metallization effect at SnO_2-ZnO heterointerfaces. A complete list of other reported studies on heterostructures-based on ZnO nanostructures is shown in Table 5.

4.5. UV activation

The sensing response of ZnO nanostructures-based gas sensors relies on the adsorbed oxygen ions. The formation of these adsorbed oxygen ions on the ZnO surface strongly depends on the working temperature. However, it is not advisable to use the sensors at high operating temperature due to the reasons, such as modification in sensor's morphology, high power consumption, and reduction of depletion layer on ZnO surface. Therefore, high sensing response, good selectivity, and fast response time should be achieved at either low operating temperature or room temperature. As high temperature creates a large depletion layer on the sensor's surface, UV activation does the same job at room temperature, thus making it one of the most effective ways to introduce a large depletion layer on the sensor's surface (Chen et al., 2016; Mishra et al., 2004). The idea is based on the generation of electron–hole pairs on the semiconductor materials, of which the band gap is less than or equal to the photon energy. On similar grounds, when UV light interacts with the ZnO nanostructures, electron–hole pairs are generated. Under atmospheric air at room temperature, this results in the adsorption of oxygen molecules on the ZnO surface, and a greater number of electrons are extracted from the conduction band of ZnO under UV light as compared to the number of extracted electrons without UV light. Thus, the formation of a depletion layer leads to an increase in the resistance and barrier height of ZnO. When reductive gas molecules interact with UV-activated adsorbed oxygen ions,
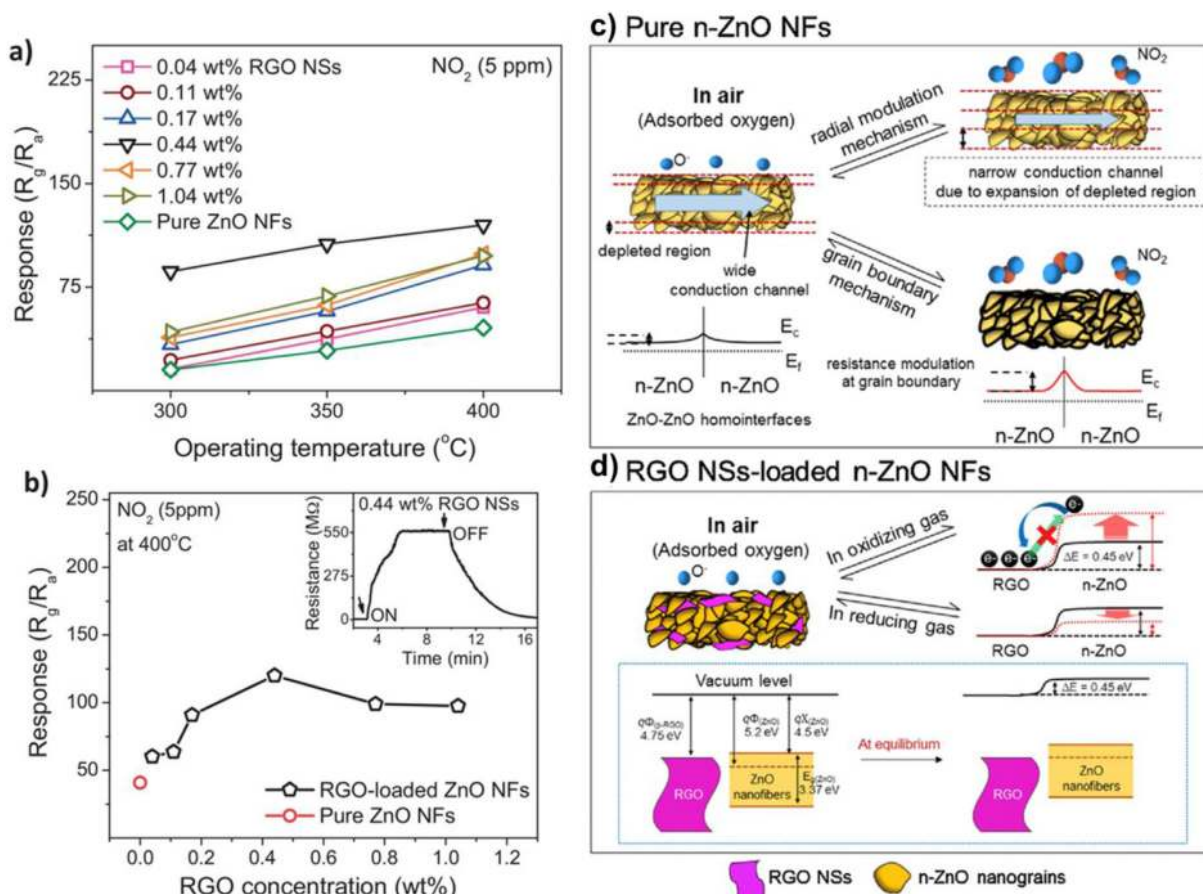
Fig. 6. (a) Sensors response of 5 ppm NO_2 with different temperatures, (b) sensors response of 5 ppm NO_2 with different RGO concentrations at 400 °C, (c–d) sensing mechanism of pure *n*-ZnO NFs and RGO-ZnO heterojunctions.
Copyright 2015, Elsevier.
Source: Reprinted from Ref. Abideen et al. (2015) with permission.

Table 4
Gas sensing response based on carbon nanomaterials/ZnO nanostructures at different temperatures.

Carbon nanomat.	Morphology (ZnO)	Synthesis method (ZnO)	Gas	Temp. (°C)	Sensing response	Res. time	Ref.
rGO	Nanoparticles	In situ method	NO_2, 5 ppm	RT	25.6% $(R_a–R_g)/R_a \times 100\%$	165	Liu et al. (2014)
Carbon	Nanofibers	Electrospinning	H_2S, 50 ppm	250	102 (R_a/R_g)	–	Zhang et al. (2018a,b,c)
MWCNTs	Nanosheets	Hydrothermal	CO, 50 ppm	100	$\sim$12.3 (R_a/R_g)	$\sim$4.9 s	Hojati et al. (2018)
Graphene	Nanoparticles	In situ method	H_2, 200 ppm	150	3.5 (R_a/R_g)	22 s	Anand et al. (2014)
CNT	Nanowires network	Flame transport	NH_3, 50 ppm	RT	430 (R_a/R_g)	–	Lupan et al. (2017)
Nanoparticle	Nanoparticles	Grafting	Acetone, 300 ppm	400	$\sim$52.5 (R_a/R_g)	–	Tian et al. (2014)
MWCNT	Nanoparticle	In situ method	NO_2, 10 ppm	300	1.023 (R_a/R_g)	93.1 s	Kwon et al. (2017)
rGO	Flower	Solution process	NO_2, 50 ppb	100	12 (R_g/R_a)	5.1 min	Liu et al. (2017)

Table 5
Gas sensing response based on MO_x/ZnO nanocomposite at different temperatures.

Metal oxide	Morphology (ZnO)	Synthesis method (ZnO)	Gas	Temp. (°C)	Sensing response	Res. time	Ref.
SnO_2	Nanorods	Hydrothermal	Triethylamine, 50 ppm	40	6.8 (R_a/R_g)	$\sim$2.0	Ju et al. (2015)
SnO_2	Nanofibers	Electrospinning	H_2, 0.1 ppm	350	78 (R_a/R_g)	74 s	Katoch et al. (2015)
CuO	Nanofibers	ALD	H_2S, 100 ppm	250	60 (R_a/R_g)	26 s	Han et al. (2019)
SnO_2	Nanorods	Hydrothermal	Ethanol, 100 ppm	275	18.1 (R_a/R_g)	3 s	Yang et al. (2019)
CuO	Nanotubular array	Spray pyrolysis	H_2S, 5 ppm	50	25% $(R_g–R_a)/R_a \times 100\%$	37 s	Li et al. (2018)
SnO_2	Film	Chemical route	H_2, 10 000 ppm	150	90% $(R_a–R_g)/R_a \times 100\%$	60 s	Mondal et al. (2014)
Fe_3O_4	3-D ordered inverse opal	Template	Acetone, 50 ppm	485	47 (R_a/R_g)	$\sim$5 s	Zhang et al. (2017a,b)

captured electrons return to the conduction band of ZnO and reduce the overall resistance (Park et al., 2016).

However, Au nanoparticles on the ZnO surface would also increase the photogenerated electron–hole pairs using resonant plasmonic effect because of more light absorption capacity of Au nanoparticles (Xu et al., 2018). As the formation of nano-Schottky barrier takes place between Au nanoparticles and ZnO surface

due to their different work functions, hot electrons have enough energy to cross the nano-Schottky barrier from Au nanoparticles to the conduction band of ZnO under the photoactivation process. This leads to the formation of a higher depletion layer on the ZnO surface because of the extraction of more electrons from the conduction band by oxygen molecules under UV light. Consequently, the sensing response is enhanced using decorated
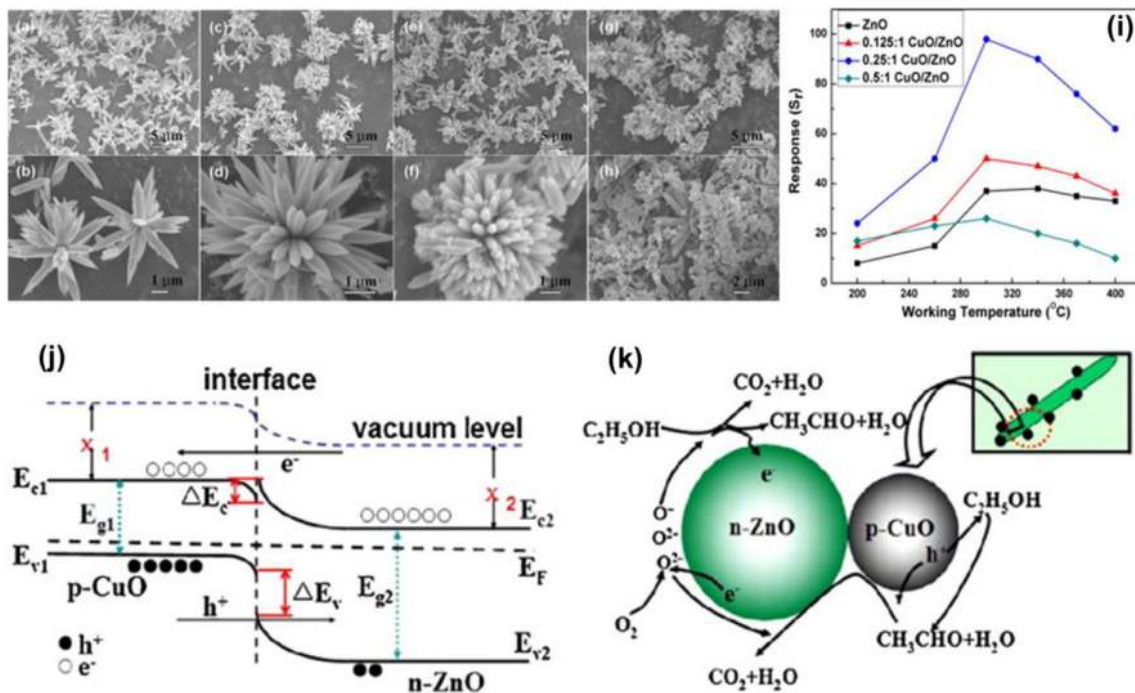
Fig. 7. FE-SEM images of all samples: (a, b) pure ZnO, (c, d) 0.125:1 CuO/ZnO, (e, f) 0.25:1 CuO/ZnO and (g, h) 0.5:1 CuO/ZnO, (i) sensing response of all samples to 100 ppm ethanol at different temperatures, and (j, k) sensing mechanism using band bending diagram.
Copyright 2014, Elsevier.
Source: Reprinted from Ref. Zhang et al. (2014) with permission.

Au nanoparticles on ZnO rather than simply using ZnO nanostructures under UV light. Drmosh et al. (2019) deposited Au nanoparticles on a rGO/ZnO heterostructured nanocomposite for room temperature H_2 detection under UV light. They performed H_2 sensing of pristine ZnO, rGO/ZnO, and Au/rGO/ZnO with and without UV light at different working temperatures, as can be seen in Fig. 8(a–d). Among all sensors, the sensor prepared based on Au/rGO/ZnO showed the highest H_2 sensing response even at room temperature, while other sensors showed a low response at high working temperature. The enhanced H_2 sensing response was due to the high surface area of ZnO, the formation of rGO/ZnO heterostructures, different work functions between Au and ZnO, and free electrons/holes generation by UV light (Fig. 8(e–g)).

Xu et al. (2018) showed a light-activated ethanol vapor sensing of Au nanoparticles-decorated ZnO nanotetrapods. In this case, an enhanced sensing was explained by photogenerated electron–hole pairs and localized surface plasmon resonance (LSPR) via decorated Au nanoparticles under UV light. Other reports representing the gas sensing response of ZnO nanostructures at room temperature under UV activation are given in Table 6.

4.6. High energy irradiation

The sensing response can also be enhanced by a post-treatment method, such as high energy irradiation on ZnO nanostructures. These irradiation sources include gamma ray irradiation, ion beam irradiation, electron-beam irradiation, and laser irradiation (Kim et al., 2019a,b,c), and the physical and chemical properties of the sensor can be modulated using these sources. While irradiating the ZnO nanostructures, energy is released in the form of core-level ionization and generation of electron–hole pairs (Ranwa et al., 2016a,b). However, irradiation-induced modification of the structural properties of the sensor occurs due to the introduction of several defects, such as oxygen vacancies and Zn interstitials. The sensing response of irradiation-induced ZnO sensor is strongly dependent on irradiation dose and radiation energy.

Kim et al. (2019a,b,c) deposited ZnO nanofibers via electrospinning technique, and irradiated them with e-beam energy of 1 MeV at different doses (50, 100, and 150 kGy) before H_2 sensing. They showed that the sensing response was improved with 150 kGy for 10 ppm H_2 and was highly selective against C_7H_8, CO, C_6H_6, and C_2H_5OH. Fig. 9(a) represents the dynamic curves of sensors with different concentrations of e-beam radiation, and Fig. 9(b) displays their calibration curve. The possible sensing mechanism of e-beam-irradiated ZnO nanofibers was attributed to the combined effect of radiation modulation, grain boundary modulation, metallization effect, and e-beam effect as shown in Fig. 9(c–f). Ranwa et al. (2016a,b) studied the impact of gamma irradiation (0, 1, 2, 5, and 10 kGy) on H_2 sensing behavior of Schottky-contacted vertically-aligned ZnO nanorods-based sensors. It was observed that the sensing response of 1 kGy gamma-irradiated ZnO nanorods was the highest for 1% H_2 at 150 °C as compared to other sensors. However, the sensing response was degraded for higher doses (5 and 10 kGy). The excellent sensing response of 1 kGy-irradiated ZnO was due to the creation of a few charge centres and defects by ionization process. Furthermore, adsorbed oxygen ions were increased on the surface of ZnO nanorods because of the generation of electrons in the ionization process. To explain further, Table 7 shows the gas sensing response based on different energy sources irradiated on ZnO nanostructures.

Conclusions and future outlook

A large number of gas sensors based on ZnO nanostructures have been discovered for the purpose of gas sensing. The main focus was to reduce the working temperature along with maintenance of high sensing response. Till date, a wide variety of ZnO nanostructures with different morphologies have been successfully synthesized via different techniques to enhance the gas
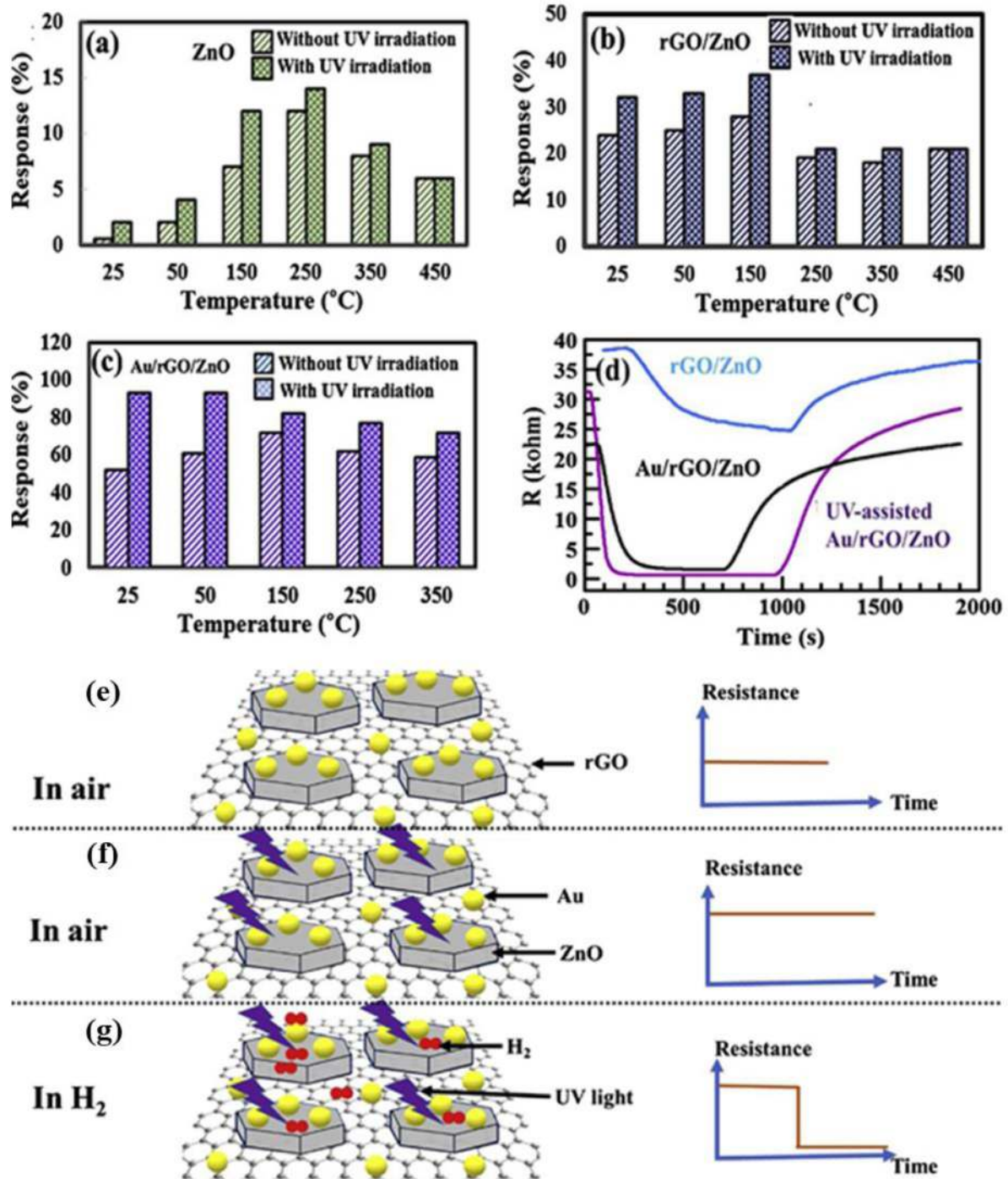
Fig. 8. (a–c) Comparison of sensing responses for all sensors with and without UV irradiation at different temperatures, (d) dynamic responses of all sensors under UV irradiation, (e–g) sensing mechanism of Au/rGO/ZnO sensor in (e) air (f) air with UV, and (g) in H_2 gas with UV irradiation.
Copyright 2019, Elsevier.
Source: Reprinted from Ref. Drmosh et al. (2019) with permission.

Table 6
Gas sensing response based on UV activation for ZnO nanostructures at room temperature.

| Second material	Morphology (ZnO)	Synthesis method (ZnO)	Gas	Sensing response	Res. time	Ref.
In_2O_3	Film	Co-precipitation	NO_2, 5 ppm	2.21, $(R_g-R_a)/R_a$	–	Espid and Taghipour (2017)
Na dopant	Nanoflowers	Solution route	Acetone, 100 ppm	3.35, (R_g/R_a)	18 s	Jaisutti et al. (2017)
Granular activated carbon	Nanorods	Hydrothermal	H_2, 200 ppm	23.2%, $(R_g/R_a)\%$	18 s	Saravanan et al. (2017)
SnO_2	Polyporous	Water bath	Formaldehyde, 10 ppm	30% $(I_a-I_g/I_g) \times 100\%$	–	Jiang et al. (2018)
SnO_2	Nanorods	Wet chemical	NO_2, 500 ppm	1266, $(R_g-R_a)/R_a$	–	Lu et al. (2012)
–	Nano-line	Chemical	H_2, 100 ppm	0.19, $(R_g-R_a)/R_a$	12 min	Fan et al. (2009)
–	Nanorods	Hydrothermal	Formaldehyde, 200 ppm	16.87, $(I_g-I_a)/I_a$	14 min	Peng et al. (2009)
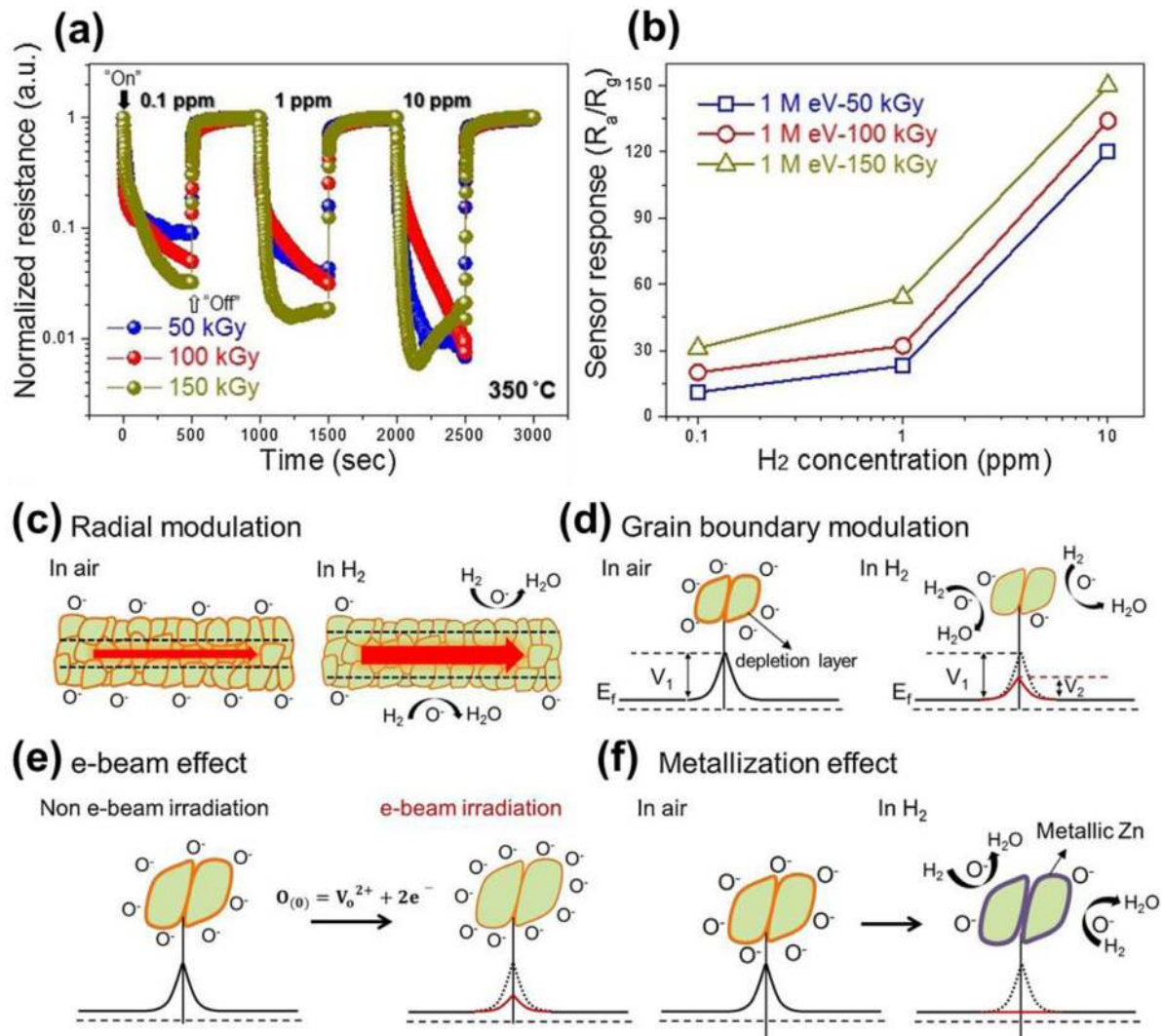
Fig. 9. (a) Normalized dynamic resistances of ZnO NF with different doses of e-beam for 0.1, 1, and 10 ppm H_2 at 350 °C, (b) calibration curves, (c–f) sensing mechanism of e-beam irradiated H_2 sensor.
Copyright 2019, Elsevier.
Source: Reprinted from Ref. Kim et al. (2019a,b,c) with permission.

Table 7
Gas sensing response based on irradiated ZnO nanostructures.

Second material	Irrad. source	Morp. (ZnO)	Syn. method (ZnO)	Gas	Temp (°C)	Sen. Res.	Res. time	Ref.
Pd	Electron beam	Nano-fibers	Electrospinning	H_2, 0.1 ppm	350	74.7 (R_a/R_g)	–	Kim et al. (2019a,b,c)
–	Au ions	Thin film	RF sputtering	H_2, 50 000 ppm	175	89.94% ($\Delta R/R_a$)%	35 s	Ranwa et al. (2016a,b)
SiO_2	Electron beam	Thin film	Sol–gel	Acetone	300	∼38 ($R_a–R_g$)/R_a	–	Nalimova et al. (2016)
–	He ions	Nanowire	Reactive vapor deposition	H_2S, 300 ppm	RT	∼9 (R_a/R_g)	–	Liao et al. (2007a,b)

sensing properties. The most common synthesis routes for ZnO nanostructures involve chemical vapor deposition, RF sputtering, hydrothermal, electrospinning, sol–gel method, template synthesis method, molecular beam epitaxy, and metal organic chemical vapor deposition. The operation of a device at low power consumption is the demand of our current scenario. Thus, in order to reduce the operating temperature, high sensing response, good selectivity, and long-term stability for a gas sensor have always been a challenge. Moreover, several attempts have been made so far to increase the gas sensing response for ZnO nanostructures. These attempts include the functionalization of noble metal nanoparticles, doping of transition metals, inclusion of carbonaceous nanomaterials, nanocomposites of different MO_x, UV activation, and post-treatment method of high energy irradiation on

ZnO nanostructures. All above-mentioned approaches efficiently reduce the working temperature of ZnO nanostructures-based gas sensors with highly sensitivity and selectivity. This reduction takes place due to the introduction of extra adsorbed oxygen ions and large change in depletion layer in the presence of target gases.

Use of noble metal nanoparticles and combination of various nanomaterials increases the cost of the sensor. The gas-sensing performance of ZnO nanostructures is limited at room temperature and can be improved by the photoactivation process. However, the final cost of photo activated gas sensor becomes higher due to the addition of UV sources and optical power detection devices. Also, this will further create a challenge for integration and reduction of the size of the device. Poor reversibility and

high response/recovery time of ZnO nanostructures based gas sensors at room temperatures are inefficient to early monitoring of flammable gases. Hierarchical nanostructures of ZnO might be promising structures where response/recovery time could be improved due to fast gas diffusion. Long term stability of ZnO nanostructures based gas sensor is another challenge attributed to changing the environmental conditions like different temperatures and different humidity levels. Such types of effects should be minimizing by means of keeping the same environmental condition near the gas sensors in real-time monitoring. The fabrication of highly selective gas sensor based on ZnO nanostructures is one of the most important tasks. However, an array of different sensing materials could be realized to improve the selectivity issue by analyzing and comparing the data from the different individual sensors. In case of flexible wearable ZnO nanostructures based gas sensors, a cracking of ZnO layer on a flexible substrate is the primary concern and needs to be rectifying these issues in the future. Thus, a cost-effective, flexible wearable, and reliable gas sensor based on ZnO nanostructures is the foremost need. In all so far discussed reports, the mechanisms for high selectivity towards a particular gas for ZnO nanostructures-based gas sensors are not convincing. Finally, we expect that our study will yield further investigation on improving highly sensitive, selective, and cost-effective ZnO nanostructures-based gas sensors at low operating temperature, and pave possible direction to better mechanism for selectivity.

References

Abideen, Z.U., Katoch, A., Kim, J.-H., Kwon, Y.J., Kim, H.W., Kim, S.S., 2015. Excellent gas detection of ZnO nanofibers by loading with reduced graphene oxide nanosheets. Sensors Actuators B 221, 1499–1507.

Alali, K.T., Liu, J., Liu, Q., Li, R., Zhang, H., Aljebawi, K., Liu, P., Wang, J., 2017. Enhanced acetone gas sensing response of ZnO/ZnCo$_2$O$_4$ nanotubes synthesized by single capillary electrospinning technology. Sensors Actuators B 252, 511–522.

Ameen, S., Akhtar, M.S., Song, M., Shin, H.S., 2012. Vertically aligned ZnO nanorods on hot filament chemical vapor deposition grown graphene oxide thin film substrate: Solar energy conversion. ACS Appl. Mater. Interfaces 4, 4405–4412.

Anand, K., Singh, O., Singh, M.P., Kaur, J., Singh, R.C., 2014. Hydrogen sensor based on graphene/ZnO nanocomposite. Sensors Actuators B 195, 409–415.

Ayana, D.G., Ceccato, R., Collini, C., Lorenzelli, L., Prusakova, V., Dirè, S., 2016. Sol-gel derived oriented multilayer ZnO thin films with memristive response. Thin Solid Films 615, 427–436.

Babu, E.S., Hong, S.K., 2015. Effect of indium concentration on morphology of zno nanostructures grown by using CVD method and their application for H_2 gas sensing. Superlattices Microstruct. 82, 349–356.

Bai, S., Guo, T., Zhao, Y., Sun, J., Li, D., Chen, A., Liu, C.C., 2014. Sensing performance and mechanism of Fe-Doped ZnO microflowers. Sensors Actuators B 195, 657–666.

Baratto, C., 2018. Growth and properties of ZnO nanorods by RF-sputtering for detection of toxic gases. RSC Adv. 8, 32038–32043.

Barthwal, S., Singh, B., Barthwal, S., Singh, N.B., 2017. ZnO-CNT nanocomposite based gas sensors - an overview. Sensor Lett. 15, 955–969.

Baruah, S., Dutta, J., 2009. Hydrothermal growth of ZnO nanostructures. Sci. Technol. Adv. Mater. 10, 013001.

Bhati, V.S., Ranwa, S., Fanetti, M., Valant, M., Kumar, M., 2018a. Efficient hydrogen sensor based on Ni-Doped ZnO nanostructures by RF sputtering. Sensors Actuators B 255, 588–597.

Bhati, V.S., Ranwa, S., Rajamani, S., Kumari, K., Raliya, R., Biswas, P., Kumar, M., 2018b. Improved sensitivity with low limit of detection of a hydrogen gas sensor based on rGO-Loaded Ni-Doped ZnO nanostructures. ACS Appl. Mater. Interfaces 10, 11116–11124.

Bhattacharyya, P., Basu, P.K., Saha, H., Basu, S., 2007. Fast response methane sensor using nanocrystalline zinc oxide thin films derived by Sol–Gel method. Sensors Actuators B 124, 62–67.

Biswas, P., Kundu, S., Banerji, P., Bhunia, S., 2013. Super rapid response of humidity sensor based on MOCVD grown ZnO nanotips array. Sensors Actuators B 178, 331–338.

Boyjoo, Y., Wang, M., Pareek, V.K., Liu, J., Jaroniec, M., 2016. Synthesis and applications of porous non-silica metal oxide submicrospheres. Chem. Soc. Rev. 45, 6013–6047.

Chang, C.-M., Hon, M.-H., Leu, I.-C., 2013. Outstanding H_2 sensing performance of Pd nanoparticle-decorated ZnO nanorod arrays and the temperature-dependent sensing mechanisms. ACS Appl. Mater. Interfaces 5, 135–143.

Chang, C.J., Lin, C.Y., Chen, J.K., Hsu, M.H., 2014. Ce-doped ZnO nanorods based low operation temperature NO$_2$ gas sensors. Ceram. Int. 40, 10867–10875.

Chen, Y., Li, X., Li, X., Wang, J., Tang, Z., 2016. UV Activated hollow ZnO microspheres for selective ethanol sensors at low temperatures. Sensors Actuators B 232, 158–164.

Chen, X., Shen, Y., Zhou, P., Zhao, S., Zhong, X., Li, T., Han, C., Wei, D., Meng, D., 2019a. NO$_2$ Sensing properties of one-pot-synthesized ZnO nanowires with Pd functionalization. Sensors Actuators B 280, 151–161.

Chen, X., Shen, Y., Zhou, P., Zhong, X., Li, G., Han, C., Wei, D., Li, S., 2019b. Bimetallic Au/Pd nanoparticles decorated ZnO nanowires for NO$_2$ detection. Sensors Actuators B 289, 160–168.

Cheng, Z., Zhou, S., Chen, T., Dong, Y., Zhang, W., Chu, X., 2012. Acetic acid gas sensors based on Ni^{2+} Doped ZnO nanorods prepared by using the solvothermal method. J. Semicond. 33, 112003.

Chia, C.H., Tsai, W.C., Chiou, J.W., 2013. Thickness effect on luminescent properties of Sol–Gel derived ZnO thin films. J. Lumin. 136, 160–164.

Cho, P.S., Kim, K.W., Lee, J.H., 2006. NO$_2$ Sensing characteristics of ZnO nanorods prepared by hydrothermal method. J. Electroceram. 17, 975–978.

Choi, K.J., Jang, H.W., 2010. One-dimensional oxide nanostructures as gas-sensing materials: Review and issues. Sensors 10.

Choi, S.-W., Kim, S.S., 2012. Room temperature Co sensing of selectively grown networked ZnOnanowires by Pd nanodot functionalization. Sensors Actuators B 168, 8–13.

Cui, J., Shi, L., Xie, T., Wang, D., Lin, Y., 2016. UV-Light illumination room temperature HCHO gas-sensing mechanism of ZnO with different nanostructures. Sensors Actuators B 227, 220–226.

Das, M., Sarkar, D., 2017. One-pot synthesis of zinc oxide-polyaniline nanocomposite for fabrication of efficient room temperature ammonia gas sensor. Ceram. Int. 43, 11123–11131.

Dey, A., 2018. Semiconductor metal oxide gas sensors: A review. Mat. Sci. Eng. B 229, 206–217.

Drmosh, Q.A., Hendi, A.H., Hossain, M.K., Yamani, Z.H., Moqbel, R.A., Hezam, A., Gondal, M.A., 2019. UV-Activated gold decorated rGO/ZnO heterostructured nanocomposite sensor for efficient room temperature H_2 detection. Sensors Actuators B 290, 666–675.

Dwivedi, P., Chauhan, N., Vivekanandan, P., Das, S., Sakthi Kumar, D., Dhanekar, S., 2017. Scalable fabrication of prototype sensor for selective and sub-ppm level ethanol sensing based on TiO$_2$ nanotubes decorated porous silicon. Sensors Actuators B 249, 602–610.

El-Shaer, A., Mofor, A.C., Bakin, A., Kreye, M., Waag, A., 2005. High-quality ZnO layers grown by MBE on sapphire. Superlattices Microstruct. 38, 265–271.

Espid, E., Taghipour, F., 2017. Development of highly sensitive ZnO/In$_2$O$_3$ composite gas sensor activated by UV-LED. Sensors Actuators B 241, 828–839.

Fan, S.-W., Srivastava, A.K., Dravid, V.P., 2009. UV-Activated room-temperature gas sensing mechanism of polycrystalline ZnO. Appl. Phys. Lett. 95, 142106.

Fan, F., Zhang, J., Li, J., Zhang, N., Hong, R., Deng, X., Tang, P., Li, D., 2017. Hydrogen sensing properties of Pt-Au bimetallic nanoparticles loaded on ZnO nanorods. Sensors Actuators B 241, 895–903.

Ganesh, R.S., Durgadevi, E., Navaneethan, M., Patil, V.L., Ponnusamy, S., Muthamizhchelvan, C., Kawasaki, S., Patil, P.S., Hayakawa, Y., 2017. Low temperature ammonia gas sensor based on mn-doped ZnO nanoparticle decorated microspheres. J. Alloys Compd. 721, 182–190.

Ghosh, R., Midya, A., Santra, S., Ray, S.K., Guha, P.K., 2013. Chemically reduced graphene oxide for ammonia detection at room temperature. ACS Appl. Mater. Interfaces 5, 7599–7603.

Gong, H., Hu, J.Q., Wang, J.H., Ong, C.H., Zhu, F.R., 2006. Nano-crystalline Cu-Doped ZnO thin film gas sensor for Co. Sensors Actuators B 115, 247–251.

Guo, J., Song, Y., Chen, D., Jiao, X., 2010. Fabrication of ZnO nanofibers by electrospinning and electrical properties of a single nanofiber. J. Dispers. Sci. Technol. 31, 684–689.

Guo, J., Zhang, J., Zhu, M., Ju, D., Xu, H., Cao, B., 2014. High-performance gas sensor based on ZnO nanowires functionalized by Au nanoparticles. Sensors Actuators B 199, 339–345.

Gupta Chatterjee, S., Chatterjee, S., Ray, A.K., Chakraborty, A.K., 2015. Graphene–metal oxide nanohybrids for toxic gas sensor: A review. Sensors Actuators B 221, 1170–1181.

Hahn, S.H., Barsan, N., Weimar, U., Ejakov, S.G., Visser, J.H., Soltis, R.E., 2003. CO sensing with SnO$_2$ Thick film sensors: role of oxygen and water vapour. Thin Solid Films 436, 17–24.

Han, C., Li, X., Shao, C., Li, X., Ma, J., Zhang, X., Liu, Y., 2019. Composition-controllable p-CuO/n-ZnO hollow nanofibers for high-performance H_2s detection. Sensors Actuators B 285, 495–503.

Hastir, A., Kohli, N., Singh, R.C., 2016. Temperature dependent selective and sensitive terbium doped ZnO nanostructures. Sensors Actuators B 231, 110–119.

He, X., Li, J., Gao, X., Wang, L., 2003. NO_2 Sensing characteristics of WO_3 thin film microgas sensor. Sensors Actuators B 93, 463–467.

Hojati, T., Ebrahimi, M., Afzalzadeh, R., 2018. Highly sensitive Co sensor based on ZnO/MWCNT nano sheet network grown via hydrothermal method. Mater. Chem. Phys. 207, 50–57.

Hübert, T., Boon-Brett, L., Black, G., Banach, U., 2011. Hydrogen sensors – a review. Sensors Actuators B 157, 329–352.

Iqbal, J., Jan, T., Ronghai, Y., 2013. Effect of Co Doping on morphology, optical and magnetic properties of ZnO 1-D nanostructures. J. Mat. Sci. Mater. El. 24, 4393–4398.

Jaisutti, R., Lee, M., Kim, J., Choi, S., Ha, T.-J., Kim, J., Kim, H., Park, S.K., Kim, Y.-H., 2017. Ultrasensitive room-temperature operable gas sensors using P-type Na:Zno nanoflowers for diabetes detection. ACS Appl. Mater. Interfaces 9, 8796–8804.

Jiang, J., Shi, L., Xie, T., Wang, D., Lin, Y., 2018. Study on the gas-sensitive properties for formaldehyde based on SnO_2-ZnO heterostructure in UV excitation. Sensors Actuators B 254, 863–871.

Jing, Z., Zhan, J., 2008. Fabrication and gas-sensing properties of porous ZnO nanoplates. Adv. Mater. 20, 4547–4551.

Ju, D.-X., Xu, H.-Y., Qiu, Z.-W., Zhang, Z.-C., Xu, Q., Zhang, J., Wang, J.-Q., Cao, B.-Q., 2015. Near room temperature, fast-response, and highly sensitive triethylamine sensor assembled with au-loaded ZnO/SnO_2 core–shell nanorods on flat alumina substrates. ACS Appl. Mater. Interfaces 7, 19163–19171.

Ju, D., Xu, H., Zhang, J., Guo, J., Cao, B., 2014. Direct hydrothermal growth of ZnO nanosheets on electrode for ethanol sensing. Sensors Actuators B 201, 444–451.

Katoch, A., Kim, J.-H., Kwon, Y.J., Kim, H.W., Kim, S.S., 2015. Bifunctional sensing mechanism of SnO_2–ZnO composite nanofibers for drastically enhancing the sensing behavior in H_2 gas. ACS Appl. Mater. Interfaces 7, 11351–11358.

Kennedy, O.W., Coke, M.L., White, E.R., Shaffer, M.S.P., Warburton, P.A., 2018. MBE Growth and morphology control of ZnO nanobelts with polar axis perpendicular to growth direction. Mater. Lett. 212, 51–53, 2018.

Kim, H.T., Lee, S.-Y., Park, C., 2017. Controls of surface morphology on Sol-Gel derived ZnO films under isothermal treatment conditions. Vacuum 143, 312–315.

Kim, J.-H., Lee, J.-H., Park, Y., Kim, J.-Y., Mirzaei, A., Kim, H.W., Kim, S.S., 2019a. Toluene- and benzene-selective gas sensors based on Pt- and Pd-functionalized ZnO nanowires in self-heating mode. Sensors Actuators B 294, 78–88.

Kim, J.-H., Mirzaei, A., Woo Kim, H., Kim, S.S., 2019b. Combination of Pd loading and electron beam irradiation for superior hydrogen sensing of electrospun ZnO nanofibers. Sensors Actuators B 284, 628–637.

Kim, J.-H., Mirzaei, A., Woo Kim, H., Wu, P., Kim, S.S., 2019c. Design of supersensitive and selective ZnO-nanofiber-based sensors for H_2 gas sensing by electron-beam irradiation. Sensors Actuators B 293, 210–223.

Kiruba Daniel, S.C.G., Kumar, A., Sivasakthi, K., Thakur, C.S., 2019. Handheld, low-cost electronic device for rapid, real-time fluorescence-based detection of Hg^{2+}, using aptamer-templated ZnO quantum dots. Sensors Actuators B 290, 73–78.

Kondalkar, V.V., Duy, L.T., Seo, H., Lee, K., 2019. Nanohybrids of Pt-functionalized Al_2O_3/ZnO core-shell nanorods for high-performance MEMS-based acetylene gas sensor. ACS Appl. Mater. Interfaces http://dx.doi.org/10.1021/acsami.9b06338.

Korotcenkov, G., Brinzari, V., Golovanov, V., Blinov, Y., 2004. Kinetics of gas response to reducing gases of SnO_2 films, deposited by spray pyrolysis. Sensors Actuators B 98, 41–45.

Kumar, R., Dossary, O.A., Kumar, G., Umar, A., 2015. Zinc oxide nanostructures for NO_2 Gas–Sensor applications: A review. Nano-Micro Lett. 7, 97–120.

Kumar, N., Dubey, A., Bahrami, B., Venkatesan, S., Qiao, Q., Kumar, M., 2018. Origin of high carrier mobility and low residual stress in RF superimposed DC sputtered Al doped ZnO thin film for next generation flexible devices. Appl. Surf. Sci. 436, 477–485.

Kumar, M., Singh Bhati, V., Ranwa, S., Singh, J., kumar, M., 2017. Pd/ZnO nanorods based sensor for highly selective detection of extremely low concentration hydrogen. Sci. Rep. 7, 236.

Kwon, Y.J., Mirzaei, A., Kang, S.Y., Choi, M.S., Bang, J.H., Kim, S.S., Kim, H.W., 2017. Synthesis, characterization and gas sensing properties of ZnO-Decorated MWCNTs. Appl. Surf. Sci. 413, 242–252.

Li, C., Du, Z., Yu, H., Wang, T., 2009. Low-temperature sensing and high sensitivity of ZnO nanoneedles due to small size effect. Thin Solid Films 517, 5931–5934.

Li, C., Li, L., Du, Z., Yu, H., Xiang, Y., Li, Y., Cai, Y., Wang, T., 2008. Rapid and ultrahigh ethanol sensing based on Au-coated ZnO nanorods. Nanotechnology 19, 035501.

Li, D., Qin, L., Zhao, P., Zhang, Y., Liu, D., Liu, F., Kang, B., Wang, Y., Song, H., Zhang, T., Lu, G., 2018. Preparation and gas-sensing performances of ZnO/CuO rough nanotubular arrays for low-working temperature H_2s detection. Sensors Actuators B 254, 834–841.

Li, Y., Tao, Z., Luo, N., Sun, G., Zhang, B., Jin, H., Bala, H., Cao, J., Zhang, Z., Wang, Y., 2019. Single-crystalline porous nanoplates-assembled ZnO hierarchical microstructure with superior tea sensing properties. Sensors Actuators B 290, 607–615.

Liao, L., Lu, H.B., Li, J.C., He, H., Wang, D.F., Fu, D.J., Liu, C., 2007a. Size dependence of gas response of ZnO nanorods. J. Phys. Chem. 111, 1900–1903.

Liao, L., Lu, H.B., Li, J.C., Liu, C., Fu, D.J., Liu, Y.L., 2007b. The sensitivity of gas sensor based on single ZnO nanowire modulated by helium Ion radiation. Appl. Phys. Lett. 91, 173110.

Liu, J., Li, S., Zhang, B., Xiao, Y., Gao, Y., Yang, Q., Wang, Y., Lu, G., 2017. Ultrasensitive and low detection limit of nitrogen dioxide gas sensor based on flower-like ZnO hierarchical nanostructure modified by reduced graphene oxide. Sensors Actuators B 249, 715–724.

Liu, L., Li, S., Zhuang, J., Wang, L., Zhang, J., Li, H., Liu, Z., Han, Y., Jiang, X., Zhang, P., 2011. Improved selective acetone sensing properties of Co-Doped ZnO nanofibers by electrospinning. Sensors Actuators B 155, 782–788.

Liu, S., Yu, B., Zhang, H., Fei, T., Zhang, T., 2014. Enhancing NO_2 gas sensing performances at room temperature based on reduced graphene oxide-ZnO nanoparticles hybrids. Sensors Actuators B 202, 272–278.

Lu, G., Xu, J., Sun, J., Yu, Y., Zhang, Y., Liu, F., 2012. UV-Enhanced room temperature NO_2 sensor using ZnO nanorods modified with SnO_2 nanoparticles. Sensors Actuators B 162, 82–88.

Lupan, O., Postica, V., Labat, F., Ciofini, I., Pauporté, T., Adelung, R., 2018. Ultrasensitive and selective hydrogen nanosensor with fast response at room temperature based on a single Pd/ZnO nanowire. Sensors Actuators B 254, 1259–1270.

Lupan, O., Schütt, F., Postica, V., Smazna, D., Mishra, Y.K., Adelung, R., 2017. Sensing performances of pure and hybridized carbon nanotubes-ZnO nanowire networks: A detailed study. Sci. Rep. 7, 14715.

Maciel, A.P., Lisboa-Filho, P.N., Leite, E.R., Paiva-Santos, C.O., Schreiner, W.H., Maniette, Y., Longo, E., 2003. Microstructural and morphological analysis of pure and Ce-Doped tin dioxide nanoparticles. J. Eur. Ceram. Soc. 23, 707–713.

Mani, G.K., Rayappan, J.B.B., 2015. A highly selective and wide range ammonia sensor— nanostructured ZnO:Co thin film. Mater. Sci. Eng. B 191, 41–50.

Maswanganye, M.W., Rammutla, K.E., Mosuang, T.E., Mwakikunga, B.W., 2017. The effect of Co and In combinational or individual doping on the structural, optical and selective sensing properties of ZnO nanoparticles. Sensors Actuators B 247, 228–237.

Mishra, S., Ghanshyam, C., Ram, N., Bajpai, R.P., Bedi, R.K., 2004. Detection mechanism of metal oxide gas sensor under UV radiation. Sensors Actuators B 97, 387–390.

Modaberi, M.R., Rooydell, R., Brahma, S., Akande, A.A., Mwakikunga, B.W., Liu, C.-P., 2018. Enhanced response and selectivity of H_2s sensing through controlled Ni doping into ZnO nanorods by using single metal organic precursors. Sensors Actuators B 273, 1278–1290.

Mohanta, S.K., Kim, D.C., Cho, H.K., Chua, S.J., Tripathy, S., 2008. Structural and optical properties of ZnO nanorods grown by metal organic chemical vapor deposition. J. Cryst. Growth 310, 3208–3213.

Mondal, B., Basumatari, B., Das, J., Roychaudhury, C., Saha, H., Mukherjee, N., 2014. ZnO–SnO_2 Based composite type gas sensor for selective hydrogen sensing. Sensors Actuators B 194, 389–396.

Mondal, K., Sharma, A., 2016. Recent advances in electrospun metal-oxide nanofiber based interfaces for electrochemical biosensing. RSC Adv. 6, 94595–94616.

Mudusu, D., Nandanapalli, K.R., Dugasani, S.R., Park, S.H., Tu, C.W., 2016. Zinc oxide nanorods shielded with an ultrathin nickel layer: Tailoring of physical properties. Sci. Rep. 6, 28561.

Nalimova, S.S., Myakin, S.V., Moshnikov, V.A., 2016. Controlling surface functional composition and improving the gas-sensing properties of metal oxide sensors by electron beam processing. Glass Phys. Chem. 42, 597–601.

Ngo, E., Venkatesan, S., Qiao, Q., 2014. Polymer photovoltaics with top metal electrode deposited by solution-processing. IEEE Trans. Electron. Dev. 61, 2957–2962.

Niu, G., Saint-Girons, G., Vilquin, B., 2018. Chapter 17 - Epitaxial systems combining oxides and semiconductors. In: Henini, M. (Ed.), Molecular Beam Epitaxy, second ed. Elsevier, pp. 377–402.

Nunes, D., Pimentel, A., Santos, L., Barquinha, P., Pereira, L., Fortunato, E., Martins, R., 2019. 2 – Synthesis, Design, and Morphology of Metal Oxide Nanostructures. Eds. Elsevier:, pp. 21–57.

Ogata, K.-i., Kawanishi, T., Maejima, K., Sakurai, K., Fujita, S., Fujita, S., 2001. Improvements of ZnO qualities grown by metal-organic vapor phase epitaxy using a molecular beam epitaxy grown ZnO layer as a substrate. Japan. J. Appl. Phys. 40, L657–L659.

Özgür, Ü., Alivov, Y.I., Liu, C., Teke, A., Reshchikov, M.A., Doğan, S., Avrutin, V., Cho, S.J., Morkoç, H.A., 2005. Comprehensive review of ZnO materials and devices. J. Appl. Phys. 98, 041301.

Park, S., Sun, G.-J., Jin, C., Kim, H.W., Lee, S., Lee, C., 2016. Synergistic effects of a combination of Cr_2O_3-functionalization and UV-irradiation techniques on the ethanol gas sensing performance of ZnO nanorod gas sensors. ACS Appl. Mater. Interfaces 8, 2805–2811.

Pati, S., Maity, A., Banerji, P., Majumder, S.B., 2013. Temperature dependent donor–acceptor transition of ZnO thin film gas sensor during butane detection. Sensors Actuators B 183, 172–178.

Peng, L., Zhao, Q., Wang, D., Zhai, J., Wang, P., Pang, S., Xie, T., 2009. Ultraviolet-assisted gas sensing: A potential formaldehyde detection approach at room temperature based on zinc oxide nanorods. Sensors Actuators B 136, 80–85.

Rai, P., Kim, Y.-S., Song, H.-M., Song, M.-K., Yu, Y.-T., 2012. The role of gold catalyst on the sensing behavior of ZnO nanorods for CO and NO_2 gases. Sensors Actuators B 165, 133–142.

Ramgir, N.S., Sharma, P.K., Datta, N., Kaur, M., Debnath, A.K., Aswal, D.K., Gupta, S.K., 2013. Room temperature H_2s sensor based on au modified ZnO nanowires. Sensors Actuators B 186, 718–726.

Ranwa, S., Barala, S.S., Fanetti, M., Kumar, M., 2016a. Effect of gamma irradiation on schottky- contacted vertically aligned ZnO nanorod-based hydrogen sensor. Nanotechnology 27, 345502.

Ranwa, S., Kulriya, P.K., Sahu, V.K., Kukreja, L.M., Kumar, M., 2014. Defect-free ZnO nanorods for low temperature hydrogen sensor applications. Appl. Phys. Lett. 105, 213103.

Ranwa, S., Kumar, M., Kulriya, P.K., Fanetti, M., Valant, M., Kumar, M., 2016b. Improvement in the sensing response of nano-crystalline ZnO-based hydrogen sensor: Effect of swift heavy ion irradiation. IEEE Sens. J. 16, 7586–7592.

Renitta, A., Vijayalakshmi, K., 2016. Highly sensitive hydrogen safety sensor based on Cr incorporated ZnO nano-whiskers array fabricated on ito substrate. Sensors Actuators B 237, 912–923.

Reshchikov, M.A., Avrutin, V., Izyumskaya, N., Shimada, R., Morkoç, H., 2007. Anomalous shifts of blue and yellow luminescence bands in MBE-grown ZnO films. Physica B 401–402, 374–377.

Rodwihok, C., Choopun, S., Ruankham, P., Gardchareon, A., Phadungdhitid-hada, S., Wongratanaphisan, D., 2019. UV Sensing properties of ZnO nanowires/nanorods. Appl. Surf. Sci. 477, 159–165.

Sansone, F.J., 1992. Fuel cell hydrogen sensor for marine applications. Mar. Chem. 37, 3–14.

Saravanan, A., Huang, B.-R., Kathiravan, D., Prasannan, A., 2017. Natural biowaste-cocoon- derived granular activated carbon-coated ZnO nanorods: A simple route to synthesizing a core–shell structure and its highly enhanced UV and hydrogen sensing properties. ACS Appl. Mater. Interfaces 9, 39771–39780.

Schütt, F., Postica, V., Adelung, R., Lupan, O., 2017. Single and networked ZnO–CNT hybrid tetrapods for selective room-temperature high-performance ammonia sensors. ACS Appl. Mater. Interfaces 9, 23107–23118.

Seiyama, T., Kato, A., Fujiishi, K., Nagatani, M., 1962. A new detector for gaseous components using semiconductive thin films. Anal. Chem. 34, 1502–1503.

Sett, D., Basak, D., 2017. Highly enhanced H_2 gas sensing characteristics of Co:ZnO nanorods and its mechanism. Sensors Actuators B 243, 475–483.

Shen, Z., Zhang, X., Mi, R., Liu, M., Chen, Y., Chen, C., Ruan, S., 2018. On the high response towards tea of gas sensors based on Ag-Loaded 3D porous ZnO microspheres. Sensors Actuators B 270, 492–499.

Shouli, B., Dianqing, L., Dongmei, H., Ruixian, L., Aifan, C., Liu, C.C., 2010. Preparation, characterization of WO_3–SnO_2 nanocomposites and their sensing properties for NO_2. Sensors Actuators B 150, 749–755.

Solís-Pomar, F., Martínez, E., Meléndrez, M.F., Pérez-Tijerina, E., 2011. Growth of vertically aligned ZnO nanorods using textured ZnO films. Nanoscale Res. Lett. 6 (524).

Song, Y., Chen, F., Zhang, Y., Zhang, S., Liu, F., Sun, P., Yan, X., Lu, G., 2019. Fabrication of highly sensitive and selective room-temperature nitrogen dioxide sensors based on the ZnO nanoflowers. Sensors Actuators B 287, 191–198.

Sui, R., Charpentier, P., 2012. Synthesis of metal oxide nanostructures by direct Sol–Gel chemistry in supercritical fluids. Chem. Rev. 112, 3057–3082.

Sun, P., Wang, W., Liu, Y., Sun, Y., Ma, J., Lu, G., 2012. Hydrothermal synthesis of 3D urchin- like A-Fe_2O_3 nanostructure for gas sensor. Sensors Actuators B 173, 52–57.

Sundara Venkatesh, P., Dong, C.L., Chen, C.L., Pong, W.F., Asokan, K., Jeganathan, K., 2014. Local electronic structure of ZnO nanorods grown by radio frequency magnetron sputtering. Mater. Lett. 116, 206–208.

Tam, K.H., Cheung, C.K., Leung, Y.H., Djurišić, .A.B., Ling, C.C., Beling, C.D., Fung, S., Kwok, W.M., Chan, W.K., Phillips, D.L., Ding, L., Ge, W.K., 2006. Defects in ZnO nanorods prepared by a hydrothermal method. J. Phys. Chem. B 110, 20865–20871.

Tian, H., Fan, H., Guo, H., Song, N., 2014. Solution-based synthesis of ZnO/Carbon nanostructures by chemical coupling for high performance gas sensors. Sensors Actuators B 195, 132–139.

Tuayjaroen, R., Jutarosaga, T., 2017. The influence of oxygen partial pressure on the shape transition of ZnO microstructure by thermal evaporation. Thin Solid Films 631, 213–218.

Umar, A., Akhtar, M.S., Al-Hajry, A., Al-Assiri, M.S., Almehbad, N.Y., 2012. Hydrothermally grown ZnO nanoflowers for environmental remediation and clean energy applications. Mater. Res. Bull. 47, 2407–2414.

Umar, A., Alshahrani, A.A., Algarni, H., Kumar, R., 2017. Cuo nanosheets as potential scaffolds for gas sensing applications. Sensors Actuators B 250, 24–31.

Urasinska-Wojcik, B., Vincent, T.A., Chowdhury, M.F., Gardner, J.W., 2017. Ultrasensitive WO_3 gas sensors for NO_2 detection in air and low oxygen environment. Sensors Actuators B 239, 1051–1059.

Vallejos, S., Gràcia, I., Lednický, T., Vojkuvka, L., Figueras, E., Hubálek, J., Cané, C., 2018. Highly hydrogen sensitive micromachined sensors based on aerosol-assisted chemical vapor deposited ZnO rods. Sensors Actuators B 268, 15–21.

Venkatesan, S., Ngo, E., Khatiwada, D., Zhang, C., Qiao, Q., 2015. Enhanced lifetime of polymer solar cells by surface passivation of metal oxide buffer layers. ACS Appl. Mater. Interfaces 7, 16093–16100.

Wales, D.J., Grand, J., Ting, V.P., Burke, R.D., Edler, K.J., Bowen, C.R., Mintova, S., Burrows, A.D., 2015. Gas sensing using porous materials for automotive applications. Chem. Soc. Rev. 44, 4290–4321.

Wang, Z.L., 2008. Splendid one-dimensional nanostructures of zinc oxide: a new nanomaterial family for nanotechnology. ACS Nano 2, 1987–1992.

Wang, W., Li, Z., Zheng, W., Huang, H., Wang, C., Sun, J., 2010a. Cr_2O_3-Sensitized ZnO electrospun nanofibers based ethanol detectors. Sensors Actuators B 143, 754–758.

Wang, C., Ma, S., Sun, A., Qin, R., Yang, F., Li, X., Li, F., Yang, X., 2014. Characterization of electrospun Pr-Doped ZnO nanostructure for acetic acid sensor. Sensors Actuators B 193, 326–333.

Wang, Z., Tian, Z., Han, D., Gu, F., 2016. Highly sensitive and selective ethanol sensor fabricated with In-Doped 3Dom ZnO. ACS Appl. Mater. Interfaces 8, 5466–5474.

Wang, C., Yin, L., Zhang, L., Xiang, D., Gao, R., 2010b. Metal oxide gas sensors: Sensitivity and influencing factors. Sensors 10.

Wei, S., Zhou, M., Du, W., 2011. Improved acetone sensing properties of ZnO hollow nanofibers by single capillary electrospinning. Sensors Actuators B 160, 753–759.

Wetchakun, K., Samerjai, T., Tamaekong, N., Liewhiran, C., Siriwong, C., Kruefu, V., Wisitsoraat, A., Tuantranont, A., Phanichphant, S., 2011. Semiconducting metal oxides as sensors for environmentally hazardous gases. Sensors Actuators B 160, 580–591, 2011.

Woo, H.-S., Kwak, C.-H., Chung, J.-H., Lee, J.-H., 2014. Co-Doped branched ZnO nanowires for ultraselective and sensitive detection of xylene. ACS Appl. Mater. Interfaces 6, 22553–22560.

Wu, F., Qiao, Q., Bahrami, B., Chen, K., Pathak, R., Mabrouk, S., Tong, Y., Li, X., Zhang, T., Jian, R., 2018a. Comparison of performance and optoelectronic processes in ZnO and TiO_2 nanorod array-based hybrid solar cells. Appl. Surf. Sci. 456, 124–132.

Wu, T., Wang, Z., Tian, M., Miao, J., Zhang, H., Sun, J., 2018b. UV Excitation NO_2 gas sensor sensitized by ZnO quantum dots at room temperature. Sensors Actuators B 259, 526–531.

Xiao, Z., Kong, L.B., Ruan, S., Li, X., Yu, S., Li, X., Jiang, Y., Yao, Z., Ye, S., Wang, C., Zhang, T., Zhou, K., Li, S., 2018. Recent development in nanocarbon materials for gas sensor applications. Sensors Actuators B 274, 235–267.

Xie, Y., Joshi, P., Darling, S.B., Chen, Q., Zhang, T., Galipeau, D., Qiao, Q., 2010. Electrolyte effects on electron transport and recombination at ZnO nanorods for dye- sensitized solar cells. J. Phys. Chem. C 114, 17880–17888.

Xu, T., Chen, Q., Lin, D.H., Wu, H.Y., Lin, C.F., Qiao, Q., 2011. Self-assembled thienylsilane molecule as interfacial layer for ZnO nanowire/polymer hybrid system. J. Photonics Energy 1, 011107.

Xu, X.L., Chen, Y., Ma, S.Y., Li, W.Q., Mao, Y.Z., 2015. Excellent acetone sensor of La- Doped ZnO nanofibers with unique bead-like structures. Sensors Actuators B 213, 222–233.

Xu, F., Ho, H.-P., 2017. Light-activated metal oxide gas sensors: A review. Micromachines 8.

Xu, F., Lv, H.-F., Wu, S.-Y., Ho, H.-P., 2018. Light-activated gas sensing activity of ZnO nanotetrapods enhanced by plasmonic resonant energy from au nanoparticles. Sensors Actuators B 259, 709–716.

Xu, J., Pan, Q., Shun, Y., Tian, Z., 2000b. Grain size control and gas sensing properties of ZnO gas sensor. Sensors Actuators B 66 (279).

Xu, J., Shun, Y.A., Pan, Q., Qin, J., 2000a. Sensing characteristics of double layer film of ZnO. Sensors Actuators B 66, 161–163.

Xu, T., Venkatesan, S., Galipeau, D., Qiao, Q., 2013. Study of polymer/ZnO nanostructure interfaces by kelvin probe force microscopy. Sol. Energy Mater. Sol. Cells 108, 246–251.

Yang, Q., Lu, Z., Liu, J., Lei, X., Chang, Z., Luo, L., Sun, X., 2013. Metal oxide and hydroxide nanoarrays: Hydrothermal synthesis and applications as supercapacitors and nanocatalysts. Prog. Nat. Sci.: Mat. Int. 23, 351–366.

Yang, C., Wu, P., Gan, W., Habib, M., Xu, W., Fang, Q., Song, L., 2016. Low temperature CVD growth of ultrathin Carbon films. AIP Adv. 6, 055310.

Yang, P., Yan, H., Mao, S., Russo, R., Johnson, J., Saykally, R., Morris, N., Pham, J., He, R., Choi, H.J., 2002. Controlled growth of ZnO nanowires and their optical properties. Adv. Funct. Mater. 12, 323–331.

Yang, X., Zhang, S., yu, Q., Zhao, L., Sun, P., Wang, T., Liu, F., Yan, X., Gao, Y., Liang, X., Zhang, S., Lu, G., 2019. One step synthesis of branched SnO_2/ZnO heterostructures and their enhanced gas-sensing properties. Sensors Actuators B 281, 415–423.

Yatskiv, R., Grym, J., 2016. Luminescence properties of hydrothermally grown ZnO nanorods. Superlattices Microstruct. 99, 214–220.

Yoo, R., Güntner, A.T., Park, Y., Rim, H.J., Lee, H.-S., Lee, W., 2019. Sensing of acetone by Al- Doped ZnO. Sensors Actuators B 283, 107–115.

Zdyb, A., Krawczak, E., Gułkowski, S., 2018. The influence of annealing on the properties of ZnO:Al layers obtained by RF magnetron sputtering. Opto-Electron. Rev. 26, 247–251.

Zeng, W., Zhu, L., Zhang, Z., Ye, Z., 2015. Fabrication of gas sensor based on mesoporous rhombus-shaped ZnO rod arrays. Sensors Actuators B 208, 112–121.

Zhang, X., Dong, Z., Liu, S., Shi, Y., Dong, Y., Feng, W., 2017a. Maize straw-templated hierarchical porous ZnO:Ni with enhanced acetone gas sensing properties. Sensors Actuators B 243, 1224–1230.

Zhang, L., Dong, B., Xu, L., Zhang, X., Chen, J., Sun, X., Xu, H., Zhang, T., Bai, X., Zhang, S., Song, H., 2017b. Three-dimensional ordered ZnO–Fe$_3$O$_4$ inverse opal gas sensor toward trace concentration acetone detection. Sensors Actuators B 252, 367–374.

Zhang, Y., Li, D., Qin, L., Zhao, P., Liu, F., Chuai, X., Sun, P., Liang, X., Gao, Y., Sun, Y., Lu, G., 2018a. Preparation and gas sensing properties of hierarchical leaf-like SnO$_2$ materials. Sensors Actuators B 255, 2944–2951.

Zhang, J., Liu, X., Neri, G., Pinna, N., 2016. Nanostructured materials for room-temperature gas sensors. Adv. Mater. 28, 795–831.

Zhang, Y., Liu, Y., Zhou, L., Liu, D., Liu, F., Liu, F., Liang, X., Yan, X., Gao, Y., Lu, G., 2018b. The role of Ce Doping in enhancing sensing performance of ZnO-based gas sensor by adjusting the proportion of oxygen species. Sensors Actuators B 273, 991–998.

Zhang, J., Lu, H., Zhang, L., Leng, D., Zhang, Y., Wang, W., Gao, Y., Lu, H., Gao, J., Zhu, G., Yang, Z., Wang, C., 2019. Metal–organic framework-derived ZnO hollow nanocages functionalized with nanoscale Ag Catalysts for enhanced ethanol sensing properties. Sensors Actuators B 291, 458–469.

Zhang, H., Xu, C., Sheng, P., Chen, Y., Yu, L., Li, Q., 2013. Synthesis of ZnO hollow spheres through a bacterial template method and their gas sensing properties. Sensors Actuators B 181, 99–103.

Zhang, Y.-B., Yin, J., Li, L., Zhang, L.-X., Bie, L.-J., 2014. Enhanced ethanol gas-sensing properties of flower-like p-CuO/ n-ZnO heterojunction nanorods. Sensors Actuators B 202, 500–507.

Zhang, J., Zhu, Z., Chen, C., Chen, Z., Cai, M., Qu, B., Wang, T., Zhang, M., 2018c. ZnO-CArbon nanofibers for stable, high response, and selective H_2s sensors. Nanotechnology 29, 275501.

Zheng, J., Jiang, Z.-Y., Kuang, Q., Xie, Z.-X., Huang, R.-B., Zheng, L.-S., 2009. Shape-controlled fabrication of porous ZnO architectures and their photocatalytic properties. J. Solid State Chem. 182, 115–121.

Zhou, T., Sang, Y., Wang, X., Wu, C., Zeng, D., Xie, C., 2018. Pore size dependent gas-sensing selectivity based on ZnO@ZIF nanorod arrays. Sensors Actuators B 258, 1099–1106.

Zhu, G., Xu, H., Liu, Y., Xu, X., Ji, Z., Shen, X., Xu, Z., 2012. Enhanced gas sensing performance of Co-Doped ZnO hierarchical microspheres to 1, 2-dichloroethane. Sensors Actuators B 166–167, 36–43.

Zhu, L., Zeng, W., 2017. Room-temperature gas sensing of ZnO-based gas sensor: A review. Sensors Actuators B 267, 242–261.

Znaidi, L., 2010. Sol–Gel-deposited ZnO thin films: A review. Mat. Sci. Eng. B 174, 18–30.

Further reading

Xu, T., Qiao, Q., 2011. Conjugated polymer–inorganic semiconductor hybrid solar cells. Energy Environ. Sci. 4 (2700).